



XCO₂ retrieval for GOSAT and GOSAT-2 based on the FOCAL algorithm

Stefan Noël¹, Maximilian Reuter¹, Michael Buchwitz¹, Jakob Borchardt¹, Michael Hilker¹, Heinrich Bovensmann¹, John P. Burrows¹, Antonio Di Noia², Hiroshi Suto³, Yukio Yoshida⁴, Matthias Buschmann¹, Nicholas M. Deutscher⁵, Dietrich G. Feist^{6,7,8}, David W. T. Griffith⁵, Frank Hase⁹, Rigel Kivi¹⁰, Isamu Morino⁴, Justus Notholt¹, Hirofumi Ohyama⁴, Christof Petri¹, James R. Podolske¹¹, David F. Pollard¹², Mahesh Kumar Sha¹³, Kei Shiomi³, Ralf Sussmann¹⁴, Yao Té¹⁵, Voltaire A. Velasco⁵, and Thorsten Warneke¹

¹Institute of Environmental Physics, University of Bremen, FB 1, P.O. Box 330440, 28334 Bremen, Germany

²Earth Observation Science, University of Leicester, LE1 7RH, Leicester, UK

³Japan Aerospace Exploration Agency (JAXA), 305-8505, Tsukuba, Japan

⁴National Institute for Environmental Studies (NIES), 305-8506, Tsukuba, Japan

⁵Centre for Atmospheric Chemistry, School of Earth, Atmospheric and Life Sciences, University of Wollongong NSW 2522 Australia

⁶Max Planck Institute for Biogeochemistry, Jena, Germany

⁷Deutsches Zentrum für Luft- und Raumfahrt, Institut für Physik der Atmosphäre, Oberpfaffenhofen, Germany

⁸Ludwig-Maximilians-Universität München, Lehrstuhl für Physik der Atmosphäre, Munich, Germany

⁹Karlsruhe Institute of Technology, IMK-ASF, Karlsruhe, Germany

¹⁰Finnish Meteorological Institute, Space and Earth Observation Centre, Tähteläntie 62, 99600 Sodankylä, Finland

¹¹NASA Ames Research Center, Atmospheric Science Branch, Moffett Field, CA 94035, USA

¹²National Institute of Water and Atmospheric Research Ltd (NIWA), Lauder, New Zealand

¹³Royal Belgian Institute for Space Aeronomy (BIRA-IASB), Brussels, Belgium

¹⁴Karlsruhe Institute of Technology, IMK-IFU, Garmisch-Partenkirchen, Germany

¹⁵Laboratoire d'Etudes du Rayonnement et de la Matière en Astrophysique et Atmosphères (LERMA-IPSL), Sorbonne Université, CNRS, Observatoire de Paris, PSL Université, 75005 Paris, France

Correspondence: S. Noël (stefan.noel@iup.physik.uni-bremen.de)

Abstract.

Since 2009, the Greenhouse gases Observing SATellite (GOSAT) performs radiance measurements in the shortwave-infrared (SWIR) spectral region. From February 2019 onward, data from GOSAT-2 are also available.

We present first results from the application of the Fast atmOspheric traCe gAs retrieval (FOCAL) algorithm to derive column-averaged dry-air mole fractions of carbon dioxide (XCO₂) from GOSAT and GOSAT-2 radiances and their validation. FOCAL has initially been developed for OCO-2 XCO₂ retrievals and allows simultaneous retrievals of several gases over both land and ocean. Because FOCAL is accurate and numerically very fast it is currently considered as a candidate algorithm for the forthcoming European anthropogenic CO₂ Monitoring (CO2M) mission, to be launched in 2025.

We present the adaptation of FOCAL to GOSAT and discuss the changes made and GOSAT specific additions. This includes particularly modifications in pre-processing (e.g. cloud detection) and post-processing (bias correction and filtering).



A feature of the new application of FOCAL to GOSAT/GOSAT-2 is the independent use of both S and P polarisation spectra in the retrieval. This is not possible for OCO-2, which measures only one polarisation direction. Additionally, we make use of GOSAT's wider spectral coverage compared to OCO-2 and derive not only XCO_2 , water vapour (H_2O) and solar induced fluorescence (SIF) but also methane (XCH_4), with the potential for further atmospheric constituents and parameters like semiheavy water vapour (HDO) and (in the case of GOSAT-2) also carbon monoxide (CO) total columns and possibly nitrous oxide (XN_2O).

Here, we concentrate on the new FOCAL XCO_2 data products. We describe the generation of the products as well as applied filtering and bias correction procedures. GOSAT-FOCAL XCO_2 data have been produced for the time interval 2009 to 2019. Comparisons with other independent GOSAT data sets reveal an agreement of long-term temporal variations within about 1 ppm over one decade; differences in seasonal variations of about 0.5 ppm are observed. Furthermore, we obtain a mean regional bias of the new GOSAT-FOCAL product to the ground based Total Carbon Column Observing Network (TCCON) of 0.56 ppm with a mean scatter of 1.89 ppm.

The GOSAT-2-FOCAL XCO_2 product is generated in a similar way as the GOSAT-FOCAL product, but with adapted settings. All GOSAT-2 data until end of 2019 have been processed. Because of this limited time interval, the GOSAT-2 results are considered to be preliminary only, but first comparisons show that these data compare well with the GOSAT-FOCAL results.

1 Introduction

Carbon dioxide (CO_2) is the most important greenhouse gas in the context of global warming (e.g. IPCC, 2013). The amount of CO_2 in the atmosphere is primarily determined by natural and anthropogenic sources and sinks but our current understanding of these sources and sinks has significant gaps (e.g., Ciais et al., 2014; Reuter et al., 2017a; Friedlingstein et al., 2019; Janssens-Maenhout et al., 2020). Retrievals of column averaged carbon dioxide (XCO_2) from the satellite sensors SCIAMACHY/ENVISAT (Burrows et al., 1995; Bovensmann et al., 1999; Reuter et al., 2010, 2011), TANSO-FTS/GOSAT (Kuze et al., 2016) and from the Orbiting Carbon Observatory-2 (OCO-2) satellite (Crisp et al., 2004; Eldering et al., 2017; O'Dell et al., 2012, 2018) have been used in over a decade to obtain information on natural CO_2 sources and sinks (e.g., Chevallier et al., 2014; Chevallier, 2015; Reuter et al., 2014b, 2017a; Schneising et al., 2014; Basu et al., 2013; Houweling et al., 2015; Kaminski et al., 2017; Liu et al., 2017; Eldering et al., 2017; Yin et al., 2018; Palmer et al., 2019) and on anthropogenic CO_2 emissions (e.g., Schneising et al., 2008, 2013; Reuter et al., 2014a, 2019; Nassar et al., 2017; Schwandner et al., 2017; Miller et al., 2019; Labzovskii et al., 2019; Wu et al., 2020; Zheng et al., 2020)

First satellite measurements of XCO_2 were performed by the Scanning Imaging Absorption Spectrometer for Atmospheric CHartography (SCIAMACHY) instrument (Bovensmann et al., 1999; Gottwald and Bovensmann, 2011; Reuter et al., 2010, 2011) on the European environmental satellite ENVISAT launched in 2002 and operating until April 2012.

Whereas greenhouse gases were only one field of application among others of SCIAMACHY, later satellite missions focused explicitly on these. In 2009, the Greenhouse gases Observing SATellite (GOSAT; Kuze et al., 2009, 2016) was launched,



followed by the Orbiting Carbon Observatory-2 (OCO-2; Crisp et al., 2017; Eldering et al., 2017; O'Dell et al., 2012, 2018) in
45 2014. Furthermore, in 2016 the Chinese TanSat mission was launched; first results have been presented by Yang et al. (2018).
Follow-on instruments to GOSAT and OCO-2 (GOSAT-2; Suto et al., 2020) and (OCO-3; Eldering et al., 2019) are in orbit
since 2018 and 2019, respectively. TanSat, GOSAT and OCO-2/3 instruments are still operating, and several different retrieval
algorithms have been developed to derive XCO_2 from their short-wave infrared (SWIR) spectra.

The main challenge for space-borne XCO_2 measurements is the required accuracy of the resulting data products as the
50 atmospheric background of XCO_2 is high compared to the variability, which is typically less than a few percent (about 2%
seasonal cycle variations in the northern hemisphere in addition to an annual increase of about 0.5% per year, see e.g. Schneis-
ing et al., 2014; Buchwitz et al., 2018). Depending on the application, even higher accuracies are needed. An accurate XCO_2
retrieval usually requires a complex retrieval method and large computational effort. This is no major problem for the number
of measurements provided by the GOSAT instruments, but even current OCO-2 retrievals require significantly larger compu-
55 tational effort. However, new missions with much higher spatial resolution and coverage are currently in preparation to answer
the challenging questions on CO_2 local and global sources and sinks in a changing climate, one amongst them is the forth-
coming European anthropogenic CO_2 Monitoring (CO2M) mission (Kuhlmann et al., 2019; Janssens-Maenhout et al., 2020),
dramatically increasing the computational power needed for retrievals.

Three years ago, Reuter et al. (2017b, c) developed the Fast atmOspheric traCe gAs retrieval (FOCAL) and applied it to
60 OCO-2 data. To show the applicability of the FOCAL method not only to OCO-2 but also to other satellite sensors, we present
in this study a new application of FOCAL to GOSAT and also some first results from an application to GOSAT-2. GOSAT-
FOCAL has several advantages over GOSAT-BESD (Heymann et al., 2015), the currently used IUP GOSAT XCO_2 retrieval,
product (Heymann et al., 2015), which provides only XCO_2 data over land. However, FOCAL is able to retrieve not only
 XCO_2 but – depending on the used spectral ranges – also other atmospheric parameters like XCH_4 , H_2O , HDO, CO and
65 N_2O . In the present study we concentrate on XCO_2 , as this is the most important (and because of its high requirements on
accuracy possibly most challenging) anthropogenic greenhouse gas.

The manuscript is organised as follows: In Section 2 we list all data sets used in this study. The retrieval algorithm is
described in section 3. Sections 4 and 5 then show the results of the retrieval and the validation. Finally, the conclusions are
given in section 6.

70 2 Data sets used

2.1 GOSAT and GOSAT-2

The Greenhouse gases Observing SATellite (GOSAT; Kuze et al., 2009) was launched in January 2009 and is still in operation.
The Thermal And Near infrared Sensor for carbon Observation (TANSO) on-board GOSAT consists of a Cloud and Aerosol
Imager (TANSO-CAI) and a Fourier Transform Spectrometer (TANSO-FTS), which measures radiances in the SWIR spectral
75 region with S and P polarisation and in the thermal infrared spectral region without polarisation with a spectral resolution of



0.2 cm^{-1} . The FOCAL retrieval uses as main input calibrated GOSAT L1B V220.220 spectra from the three SWIR bands (around 0.76, 1.6 and $2.0 \mu\text{m}$) of TANSO FTS.

GOSAT-2 (Nakajima et al., 2017; Suto et al., 2020) was launched in October 2018 and comprises a similar instrumentation as GOSAT. The GOSAT-2 FTS has the same spectral resolution but an extended spectral range for SIF and CO retrievals.

80 We use calibrated GOSAT-2 L1B SWIR data V101.101.

Both GOSAT and GOSAT-2 perform point measurements with a spatial resolution (footprint diameter) of about 10 km. For both instruments, we use a tabulated instrumental line shape (ILS) with a kernel width of 15 cm^{-1} . For GOSAT this has been generated by a theoretical formula parameterising a “real-world” FTS instrument (see e.g. formula 5.21 in Davis et al., 2001), which depends on the maximum optical path difference (MOPD, $\pm 2.5 \text{ cm}$ for GOSAT) and the size of the instantaneous field of view (IFOV, 15.8 mrad for GOSAT). The same formula has been used by Heymann et al. (2015). This ILS is symmetric and the same for S and P polarisation.

For GOSAT-2, we use a preliminary tabulated ILS provided by JAXA and generated on 16 January 2020, which is different for S and P polarisation and asymmetric, especially in the SWIR-1 band. Meanwhile, this ILS has been officially released and is available via the NIES web site.

90 2.2 Reference Spectra and External Databases

For the retrieval several reference spectra and databases are used.

The solar spectrum used in the forward model is based on a high resolution solar transmittance spectrum (O’Dell et al., 2012) in combination with an ISS solar reference spectrum (Meftah et al., 2018). For the SIF retrieval we used a chlorophyll fluorescence spectrum by Rascher et al. (2009), which has been scaled to $1.0 \text{ mW/m}^2/\text{sr}/\text{nm}$ at 760 nm.

95 We use tabulated cross sections at a 0.001 cm^{-1} sampling based on HITRAN2016 (Gordon et al., 2017) and the absorption cross section database ABSCO v5.0 (Benner et al., 2016; Devi et al., 2016) from the NASA (National Aeronautics and Space Administration) ACOS/OCO-2 project.

Surface elevation, surface roughness and surface type are derived from the Global Multi-resolution Terrain Elevation Data (GMTED2010; Danielson and Gesch, 2011) of the U.S. Geological Survey (USGS) and the National Geospatial-Intelligence Agency (NGA) at a spatial resolution of 0.025° . Meteorological information (pressure, temperature, water vapour profiles) is obtained from ECMWF (European Centre for Medium-range Weather Forecasts) ERA 5 model data (Hersbach et al., 2020), which are available every 1 hour on a 0.25° horizontal grid and on 137 altitude layers.

100 We use XCO_2 data from the CarbonTracker (CT) model CT2019 and CT-NRT v2020-1 (Jacobson et al., 2020a, b) and data from the Total Carbon Column Observing Network (TCCON, see e.g. Wunch et al., 2011) in the context of the bias correction database (see section 2.3). TCCON data are also used for validation (see section 5). Table 1 lists the TCCON stations which provided data for the present study.

XCO_2 a-priori profiles are derived using the 2018 version of the simple empirical CO_2 model SECM (Reuter et al., 2012). In the context of validation, we use the 2020 version of SECM. XCH_4 a-priori data are from the simple CH_4 climatological model SC4C2018 developed and used by Schneising et al. (2019) and briefly described by Reuter et al. (2020).



110 For CO₂ we use the “synth” a-priori error covariance matrix described by Reuter et al. (2017b). For H₂O, we use the same error covariance matrix as Reuter et al. (2017b), but scaled by a factor of 5 to reduce the dependencies of the retrieval results on the a-priori. For CH₄, for convenience, we scale the CO₂ matrix to result in an XCH₄ uncertainty of 45 ppb, which is considered to be a reasonable estimate. Note that only the matrices are scaled, not the a-priori values.

2.3 The “true” database

115 Quality filtering and bias correction usually require the knowledge of a “true” (in this case XCO₂) value. For this, we do not simply use model data as truth, as one aim of XCO₂ products is to improve models. Another method is to take ground-based TCCON measurements as basis for a bias correction. However, although TCCON measurements are very accurate, they are only available at certain locations and are therefore more suited for validation.

Our choice is therefore to use a data base generated from a combination of TCCON measurements and CarbonTracker (CT) model data for a reference year (2018 for GOSAT, 2019 for GOSAT-2).

This database is produced in the following way: As a first step, we determine from the CT data global daily 3D maps close to 13:00 local time (i.e. GOSAT and GOSAT-2 equator crossing time). We reduce the altitude grid to five layers with the same dry-air sub-columns, i.e. the same amount of particles, and interpolate the data from the native CT horizontal resolution of 3° × 2° to 0.5° × 0.5°. Then we determine from the TCCON data daily mean values (XCO₂^{TCCON}) for 13 h ± 2 h local time. Next, we select collocated CT data and correct them for the TCCON averaging kernels, resulting in a TCCON corrected CT value at the TCCON location (XCO₂^{CT}). The application of the averaging kernels corrects for different vertical resolutions/sensitivities (see e.g. Rodgers and Connor, 2003; Wunch et al., 2010). We look for contiguous regions where CT data differ by less than 0.75 ppm from XCO₂^{CT}; these data are then used for the “true” database. The result are daily maps containing CO₂ data for five vertical sub-layer altitudes. The spatial coverage is usually not global and varies from day to day. There are typically more data in the southern hemisphere during the second half of the year. When comparing with GOSAT or GOSAT-2 measurement results, the “true” XCO₂ is then computed from the CO₂ layers of the true database, considering the retrieval’s averaging kernels.

Specifically, we use here for GOSAT CT2019 data in combination with TCCON GGG2014 (see Tab. 1) for 2018. For GOSAT-2 we also use TCCON GGG2014 data, but need to rely on CT-NRT v2020-1 for 2019. Because the CT NRT data are not yet available for the whole year 2019, the GOSAT-2 “true” database does not cover the whole year; there are essentially no data after August 2019. This is a limiting factor for GOSAT-2, especially because this also means that data in the southern hemisphere are less present in the 2019 database.

Please note that the “true” database does not contain any TCCON data - it only contains CT data which were confirmed by TCCON, but individual values may differ by up to 1.5 ppm. This is why a later validation with TCCON still makes sense.

140 2.4 GOSAT Level 2 Products

To assess the quality of the newly created GOSAT-FOCAL XCO₂ products, they have been compared with several other well-established GOSAT Level 2 data sets (see section 5). The GOSAT BESD v01.04 product from IUP (Heymann et al., 2015) is a



near-real time product generated in the context of the Copernicus Atmospheric Monitoring Service (CAMS, <https://atmosphere.copernicus.eu/> (last access: 30-July-2020)) project. It is available from 2014 onward. The GOSAT RemoTeC v2.3.8 product
145 from SRON (Butz et al., 2011) and the full-physics GOSAT product from the University of Leicester v7.3 (Cogan et al., 2012)
were generated in the context of the Copernicus Climate Change Service (C3S, <https://climate.copernicus.eu/>; last access: 30-
July-2020) and cover the GOSAT time series from 2009 until end of 2019. The recently released NASA GOSAT ACOS v9r
product (O'Dell et al., 2012, 2018; Kiel et al., 2019) is also available for the years 2009 to 2019. The operational GOSAT
XCO₂ product v02.95 (bias corrected) from NIES currently ends in August 2020. The BESD product contains only XCO₂
150 data over land, all other products are available for water and land surfaces.

3 Retrieval Algorithm

The retrieval is performed in three main steps: Pre-processing, processing and post-processing. These are described in the following sub-sections.

3.1 Pre-Processing

155 During pre-processing all required input data for the main processing step are collected. Furthermore, a first filtering of data is performed to reduce processing time.

The pre-processing procedure is largely based on the pre-processing as present in the BESD GOSAT product (Heymann et al., 2015). The sequence of pre-processing activities is as follows:

1. Extraction of measured spectra, geolocation and information on quality and measurement modes (e.g. gain, scan direc-
160 tion) from the GOSAT LIB product.
2. Estimation of instrument noise and cloud parameters.
3. Filtering for data quality, latitudes, solar zenith angle, signal-to-noise ratio and clouds (see Tab. 2 for settings).
4. Extraction of surface type, elevation and roughness derived from the surface database for each measurement.
5. Addition of corresponding meteorological information (pressure, temperature, dry-air column and water vapour profiles)
165 for the time and place of the measurements. This includes a correction for surface elevation, i.e. model profiles are extended / cut according to the value from the surface database.
6. Add a-priori gas profiles for each measurement (CO₂ from SECM, CH₄ from SC4C, H₂O from meteorology). For
170 GOSAT-2, also a-priori profiles for CO and N₂O are added. The latter do not depend on geolocation; they are based on the tropical reference atmosphere from Anderson et al. (1986), scaled to column average values of XCO = 0.1 ppm and XN₂O = 330 ppb.



Because FOCAL is a fast algorithm and the number of GOSAT and GOSAT-2 measurements is much less than for OCO-2, we chose to set the pre-processing filters relatively relaxed and to apply the quality filtering mostly in the post-processing. As can be seen from Fig. 1 about two thirds of the measurements are filtered out during pre-processing.

3.1.1 Noise Estimate

175 Similar to Heymann et al. (2015) the spectral noise is initially assumed to be independent from wavenumber for each band. It is estimated from the standard deviation of the real part of the “dark” off-band signal (i.e. the first 500 spectral points in each band). In a later step (see Section 3.2.1) this noise will be modified to account for additional forward model errors and overall scaling.

3.1.2 Cloud Filter

180 The cloud filtering is based on two physical properties of clouds: clouds are (usually) bright and clouds are high (higher than the surface) so that little water vapour is above them. In the pre-processing these properties are described by two quantities: cloud albedo and water vapour path. These are derived for each spectrum as described in Heymann et al. (2015). The cloud albedo for each band is estimated from the mean reflectance L within a spectral range outside the absorption. L is determined from the mean radiance I , the mean irradiance I_0 and the solar zenith angle α via:

$$185 \quad L = \frac{\pi I}{I_0 \cos \alpha} \quad (1)$$

The specific wavenumber ranges and irradiance values used for filtering are given in Tab. 3.

The water vapour path is determined from a spectral region with strong water vapour absorption in the SWIR-3 band (see Tab. 3). It is given by the ratio between the median radiance and the median of the estimated noise in this spectral range.

190 A ground pixel is assumed to be cloudy if either the cloud albedo in one of the bands or the water vapour path exceeds the thresholds given in Tab. 2.

3.2 Processing

The processing is based on the Fast atmospheric trace gas retrieval (FOCAL) algorithm which is described in detail in Reuter et al. (2017c). A first successful application of this algorithm to OCO-2 data is given in Reuter et al. (2017b). Therefore, we only summarise the main features of the algorithm here and point out the differences to the OCO-2 application.

195 FOCAL approximates modifications of the direct light path due to scattering in the atmosphere by a single scattering layer, which is characterised by its height (pressure level), its optical thickness and an Ångström parameter which describes the wavenumber dependence of scattering. The layer height is normalised to the surface pressure. Furthermore, Lambertian scattering on the surface is considered. For atmospheric scattering processes an isotropic phase function is assumed. With this approximation, the FOCAL forward model is essentially an analytical formula; it uses pre-calculated and tabulated cross
200 sections such that calculations can be performed considerably fast. The inversion of the forward model is based on optimal estimation (Rodgers, 2000) and uses the Levenberg-Marquardt-Fletcher method (Fletcher, 1971) to minimise the cost function.



The OCO-2 retrieval of Reuter et al. (2017b, c) uses four fit windows in the NIR (near-infrared) and SWIR spectral range to derive the atmospheric parameters XCO_2 , water vapour and SIF. In contrast to OCO-2, GOSAT and GOSAT-2 cover a wider spectral range and provide spectra in two polarisation directions referred to as S and P. Therefore, we treat in our retrieval both polarisation directions as independent spectra opposed to the average of both as usually used in other GOSAT retrievals (see e.g. Butz et al., 2011; Cogan et al., 2012; O'Dell et al., 2012). However, recently Kuze et al. (2020) presented a methane retrieval for GOSAT based on an algorithm from Kikuchi et al. (2016), which also makes use of both polarisation directions. Furthermore, the FOCAL fitting windows (see Tab. 4) have been adapted to the specific GOSAT(-2) spectral bands such that in addition also other atmospheric constituents and parameters like HDO and (in the case of GOSAT-2) also CO total columns and possibly XN_2O can be retrieved. This results in six fitting windows for GOSAT and eight windows for GOSAT-2 for each polarisation. The retrieval is performed on a wavenumber axis.

Because of the large number of target gases and spectral bands the retrieval requires various state vector elements. These are listed together with the fit windows, from which they are determined, and their a-priori values and uncertainty ranges in Tab. 5 for GOSAT and GOSAT-2.

For GOSAT, the retrieval determines CO_2 , CH_4 and H_2O on 5 layers with same number of air particles, from which then the column average values XCO_2 , XCH_4 and XH_2O are calculated. Furthermore, solar induced fluorescence (SIF) is determined by scaling of a corresponding reference spectrum.

Instead of the HDO column, we fit a scaling factor for the relative abundance of HDO compared to H_2O , δD , which is defined as:

$$\delta D = \frac{R_{\text{meas}}}{R_{\text{VSMOW}}} - 1 \quad (2)$$

where R_{meas} is the ratio of the measured HDO and H_2O columns, $R_{\text{VSMOW}} (= 3.1152 \times 10^{-4})$ is the corresponding value for Vienna Standard Mean Ocean Water (VSMOW). δD is usually given in units of per-mill.

$\delta D = 0\%$ corresponds to HDO concentrations as in VSMOW, $\delta D = -1000\%$ to no HDO. We assume the same profile shape for HDO as for H_2O . For GOSAT-2, we also fit scaling factors to (fixed) CO and N_2O profiles.

As mentioned above, atmospheric scattering is considered in FOCAL by a single scattering layer, which is described by three parameters (height, optical depth and Ångström coefficient). As scattering is different for S and P polarised light, we fit two independent layers for S and P.

In addition, we determine in each fit window (independently for S and P) a polynomial background function describing the surface albedo. For this we use second order polynomials except for the small SIF windows (no. 1) where a linear function is sufficient.

The GOSAT data files only contain a fixed spectral axis. As e.g. described in Heymann et al. (2015), the spectral calibration of GOSAT changes especially at the begin of the mission with time. This change can be corrected by a spectral scaling factor. We determine this overall scaling factor by a spectral fit in the SIF window before the retrieval. So far, this spectral pre-fitting seems to be unnecessary for GOSAT-2. In the retrieval, we then additionally consider for both GOSAT and GOSAT-2 possible



235 additional spectral shifts and squeezes in each fit window by corresponding state vector elements, but the influences of these
spectral changes on the results is rather small.

3.2.1 Noise Model

The noise N derived from the off-band signal is only an estimate. It does not consider a possible wavenumber dependence of
the noise within one spectral band. Furthermore, a potential error of the forward model needs to be considered. In the optimal
240 estimation method this can be achieved by including the forward model error in the measurement error covariance. For this,
we define a scaling factor s for the estimated noise and the quantity δF , which denotes the relative error of the forward model.
The forward model error is proportional to the continuum radiance outside the absorption I , which is estimated from the 0.99
percentile of the measured radiance at the edge of each fit window. The quantities δF and s are determined using the approach
described in (Reuter et al., 2017b), i.e. by running the retrieval for a representative subset of data and then fitting the function

$$245 \quad RSR(NSR) = \sqrt{(s \ NSR)^2 + \delta F^2} \quad (3)$$

to binned values of the residual-to-signal ratio (RSR) as function of the noise-to-signal ratio (NSR). RSR is defined as the
standard deviation of the retrieved spectral residual in each fit window divided by the continuum signal I ; NSR is the standard
deviation of the noise divided by I .

With the method described in Reuter et al. (2017c) it is also possible to define a 2σ -outlier limit based on NSR and RSR
250 data, which will be used to filter out too noisy data during post-processing (see section 3.3). This is parameterised by a second
order polynomial as a function of the uncorrected NSR

$$f_N(NSR) = a_0 + a_1 \ NSR + a_2 \ NSR^2 \quad (4)$$

which is added to the RSR function of Eq. (3). The coefficients a_i are determined via a fit. To avoid extrapolation, f_N is set to
the edge values outside the fitting range.

255 In order to cover the varying signal over the year, we base the noise model fits on data from one day per month for one
reference year. For GOSAT, we take from December 2017 to November 2018 (as there are only few GOSAT data available in
December 2018). For GOSAT-2 we use data from February 2019 to December 2019. In the case of GOSAT-2 we further restrict
the input data for the noise model parameter fit to data over land because some of the data over water show an unexpected
behaviour (low RSR in case of large NSR), which needs further investigation. In this sense, the current GOSAT-2 noise model
260 is considered to be preliminary and may need some refinement in the future.

Figs. 3 to 6 show the noise model results for GOSAT and GOSAT-2. The orange line gives the fitted RSR function, the
red line the outlier limit. The derived values from the noise model are given in Tab. 6 and 7 for GOSAT and GOSAT-2. The
forward model errors δF are on average slightly larger for GOSAT-2 than for GOSAT. In the SWIR, values similar to OCO-2
are obtained, but in the NIR the OCO-2 δF is typically smaller (about 0.003). This indicates that for GOSAT and GOSAT-2
265 instrumental/calibration effects seem to impact the radiance errors more in the NIR than in the SWIR.



3.3 Post-Processing

The purpose of post-processing is to filter out invalid data and to perform a bias correction for the products. The current post-processing focuses on XCO₂. The post-processing is performed in several steps, namely:

1. Basic filtering based on physical knowledge.
- 270 2. Filtering out low quality data using parameters / limits determined using a random forest classifier.
3. Application of a bias correction using a random forest regressor.
4. Additional filtering out of data with too large bias correction.

These steps are described in the following subsections.

3.3.1 Basic filter

275 The basic filtering removes measurements where the retrieval does not converge or where the quality of the fit results is too low. We consider this to be the case if the χ^2 calculated over all fit windows is larger than 2 or if for at least one of the fit windows the RSR outlier limits (see section 3.2.1) are exceeded. Furthermore, we apply some initial filters for nonphysical values on the derived scattering parameters (i.e. layer height outside the atmosphere, Ångström coefficient not within [1,5]). We also limit the maximum allowed optical depth of the scattering layer to 0.02 to filter out too thick clouds or aerosol amounts
280 and use a maximum allowed XCO₂ error of 2 ppm. As described by Reuter et al. (2017c), FOCAL simulates scattering only for an isotropic phase function. The prominent forward peak, usually existing for Mie scattering phase functions of cloud and aerosol particles does basically not modify the lightpath. As FOCAL's optical depths of the scattering layer do not include this forward peak, these optical depths are much smaller than optical depths including a strong forward peak while having a similar influence on the light path modification (see discussion in the publication of Reuter et al. (2017c)). The maximum value of
285 0.02 for the layer optical depth should therefore not be interpreted as e.g. an aerosol optical depth.

The limits for the optical depth of the scattering layer and the XCO₂ error are somewhat arbitrary and actually result from visual inspection of the retrieval results. However, they are only intended as a first rough quality filter to facilitate later filter and bias correction methods, which will partly use the same parameters (see below). The detailed choice of these limits is therefore considered uncritical for the final results.

290 The above mentioned filter parameters and limits (see Tab. 8) are applied to both land and water surfaces and are the same for GOSAT and GOSAT-2, except for the RSR outlier limit which has been determined individually for each instrument. Figs. 1 and 2 show exemplarily how many data points are filtered out in this step.

3.3.2 Random forest filter

In the next step, data are filtered out based on their expected XCO₂ bias i.e. the difference to a “true” XCO₂. Of course,
295 this true XCO₂ value is normally not known. We therefore use the “true” reference database (as described in section 2.3)



to train a random forest classifier (Pedregosa et al., 2011) to identify those variables which would remove – in combination with a corresponding random forest database – a pre-described percentage p of data based on their XCO_2 bias. This is done independently for data over land and water. Note that we are only interested here in the XCO_2 bias on top of an overall global bias as the latter will be handled via the bias correction.

300 We determine the list of relevant variables and the random forest database for the filtering in the following way: We use the (uncorrected) results of the retrieval for the reference and apply the basic filtering as described in section 3.3.1. Then, the subset of these data is selected which has a corresponding “true” value in the reference database. For these data we determine the XCO_2 bias (measurement - reference XCO_2) and subtract the monthly global median of this bias. We then sort the data according to this bias and flag those p percent of data with the highest absolute bias values as “bad”. The random forest classifier
305 is then trained by using randomly 90% of these data as input. The training is done in two iterations: First, with a complete set of possible input variables (“features”) and output variables (“estimators”); then, using only a reduced set consisting of the 10 best features/estimators (i.e. those with highest random forest score of the first run). The random forest classifier then decides for each measurement based on these 10 variables if it is filtered out or not.

The initial list of possible features/estimators includes essentially all quantities available after the retrieval, including viewing
310 angles, surface properties and continuum signal for each fit window. Furthermore, the retrieved values of the state vector elements and their errors are included in this list as well as averaging kernels for the profiles. We explicitly exclude the geolocation of the measurement (latitude, longitude) and the retrieved values (but not the errors) for the data products we are interested in, i.e. the gases and SIF. This is to avoid e.g. the filtering out of certain geographical regions or removing all points with high XCO_2 values. However, we include as possible filter variable the gradient of the retrieved CO_2 profile (i.e. the
315 difference between the two lowermost layers) as this has shown to be a suitable quantity.

The original number of candidate variables presented to the random forest classifier is quite high (193 for GOSAT and 246 for GOSAT-2) as can be seen from Figs. 7 and 8 (top left plots), but there are only few with a high relevance. The ten best variables selected partly differ for land and water surface (as shown in the middle and left top panels), but they usually comprise scattering parameters, polynomial coefficients, spectral corrections and some XCO_2 related parameters.

320 The other 10% of the input data are used to test the performance of the classifier. The results from this test and other cross-validation activities indicate, that the random forest classification is – depending on surface – only accurate in about two thirds of the cases. This means that the filtering also removes possibly valid data points and does not remove all possibly bad ones. However, we do not expect a perfect classification, because it is not possible to describe all inter-dependencies via the set of input features.

325 To obtain a high quality of the remaining XCO_2 data, we therefore need to filter out quite a large percentage of data (and perform an additional filtering at a later time, see below). For future data products further investigations are planned to improve the performance of the classifier, e.g. by providing additional features from combination of existing ones (like the already used CO_2 gradient). The percentage p of data to be filtered out is usually a trade-off between data quality and remaining amount of data. In the present case a 50% limit has been selected. Actually, as can be seen from Figs. 1 and 2, the relative amount of data
330 filtered out via the random forest classifier is not exactly 50% of the data remaining after the previous filters.



3.3.3 Bias correction and filtering

Reuter et al. (2017c) use for OCO-2 a bias correction based on the “small area approximation”(see also O’Dell et al., 2018; Kiel et al., 2019), which assumes that the variation of XCO_2 within a small area is small. This is not possible for GOSAT and GOSAT-2 because of their sparse sampling. We therefore follow a different approach here.

335 For the bias correction we use as input the same data set as for the random forest filter, but with this filter applied. 50% of the resulting data set is then used to train a random forest regressor, which aims to minimise the “true” XCO_2 bias (without global median subtracted) as function of the specified features. To create the bias correction database and the corresponding list of best features we again run the training twice, first with the full list (the same as for the filter) and then with the top ten features. Again, we use different corrections for land and water. The resulting parameters and their performance are shown
340 in the bottom panels of Figs. 7 and 8. The bias correction selects similar best features as the filter, but not exactly the same quantities in the same sequence.

During application of the bias correction, the random forest regressor estimates the XCO_2 bias based on the values of the input variables. This bias is then subtracted from the retrieved value. Application of the bias correction to the training data set and the other 50% of the input data shows a comparable reduction of the XCO_2 scatter, which is an indication for a good
345 performance (e.g. no over-fitting) of the regressor.

Currently, there is only a bias correction for XCO_2 , but in principle this method is applicable also to other quantities depending on the availability of a corresponding “true” database.

After the bias correction there are still a few outliers left in the XCO_2 data. These are filtered out by an additional filter on the derived XCO_2 bias. The limits for this filter are the global median bias for test data set ± 2 ppm. the median bias is
350 different for land and water surfaces and also for GOSAT and GOSAT-2. The actual limits are given in Tab. 9. The value 2 ppm is estimated from visual inspection of the data. Figs. 1 and 2 show that typically less than 1–2% of the remaining data (less than 0.1% of all) are affected by this last filter.

4 Results

The FOCAL retrieval has been applied to all GOSAT and GOSAT-2 measurements until end of 2019. On average, FOCAL
355 needs 22 s with 6 iterations for the processing of one GOSAT ground pixel. For GOSAT-2 numbers are slightly larger (28 s/7 iterations) because of the additional fit windows and state vector elements. All performance values are given for a single core of an Intel Xeon E5-2667v3 CPU (3.2 GHz). These numbers are actually about one magnitude larger than the ones given in Reuter et al. (2017b, c) for the FOCAL application to OCO-2. This is because we use for GOSAT(-2) separate S and P polarisation spectra and more retrieved variables, which requires more and larger fit windows. For each of these fit windows
360 and parameters, weighting functions have to be calculated, which involves a convolution with the ILS. This convolution is the most time consuming part of the FOCAL retrieval. This is even more relevant for GOSAT(-2), because the FTS ILS is in principle sinc-shaped, i.e. it has a sharp peak in the centre but wide wings, which requires a large kernel width (in our case 15 cm^{-1} for the convolution).



Figs. 9 to 12 show examples for measured and fitted nadir mode radiance spectra for GOSAT and GOSAT-2 over land in the
365 different fitting windows. Since the difference between measured and modelled spectra is small and thus hard to see, we show
in Figs. 13 to 16 the corresponding residuals and the estimated noise. The residuals are on the order of magnitude of the noise,
which is slightly higher for P polarisation than for S polarisation. Some small spectral structures are visible in the residuals,
they appear more clearly in the smoothed residuals (convoluted with a 21 pixel boxcar), e.g. for GOSAT and GOSAT-2 in
the $O_2(A)$ band (window 2), and some broadband oscillations in window 4 and 5 for GOSAT-2. These features are present in
370 both S and P polarisations and occur also in other measurements, so they seem systematic. A reduction of these features could
possibly further improve future products.

In Fig. 17 some statistical information about the GOSAT-FOCAL data products is given. A time series for the number of
valid data is given in the top plot. In the recent years, about 5–6% of the available measurements could be transferred to
valid XCO_2 data. The number of valid data points increases from 2009 to 2019. This is mainly due to an increase in the data
375 over water, which is most likely related to optimisations in GOSAT operations (better use of glint geometry) over water. As
expected, the mean global XCO_2 shown in the middle plot increases with time. Global mean values over water are typically
slightly higher than over land; this is most likely a spatial sampling issue. The observed XCO_2 variability (standard deviation,
bottom plot) is larger over land which is attributed to influences of surface elevation. For GOSAT-2, only retrieved data from
2019 are available so far. The total amount of available measurements is about 2.8 million, compared to about 3.5 million
380 GOSAT measurements in 2019. Only about 3% of the GOSAT-2 data remain after all filtering / post-processing, which is
roughly half of the corresponding number for GOSAT (but similar to the first year of GOSAT). As can be seen from Fig. 2
more GOSAT-2 data are filtered out due to failed or bad convergence and by the RSR outlier limits than for GOSAT (Fig. 1).
Future improvements of the GOSAT-2 calibration or the noise model could possibly help here.

For further analyses, we have generated monthly maps on a $5^\circ \times 5^\circ$ grid. Example plots for the months April and August
385 2019 (begin/end of the growing season) are shown in Fig. 18 for GOSAT and in Fig. 19 for GOSAT-2. The data are not filtered
for low amounts of input data in the grid points, which may explain some individual outliers in the plots. Overall, the spatial
patterns observed by GOSAT and GOSAT-2 look reasonable. The north–south gradient in XCO_2 is visible with different sign
in April and August for both instruments. The spatial coverage of the GOSAT-2 data is lower than for GOSAT, because more
data are filtered out (see above). This seems to affect especially regions like the northern part of Africa.

390 5 Verification and Validation

For the verification and validation of the GOSAT and GOSAT-2 FOCAL products we perform a comparison with various
reference data sets (see section 2), namely:

- The GOSAT BESD v01.04 product from IUP (referred to as “BESD” later).
- The GOSAT ACOS v9r product from NASA (referred to as “ACOS” later).
- 395 – The GOSAT UoL_FP v7.3 product from the University of Leicester (referred to as “UoL” later).



- The GOSAT RemoTeC v2.3.8 product from SRON (referred to as “SRON” later).
- The GOSAT operational product v02.95 (bias corrected) from NIES (referred to as “NIES” later).
- Collocated TCCON GGG2014 data (referred to as “TCCON” later).

For the comparisons, all data have been adjusted using the same a-priori (SECM2020).

400 Since all GOSAT products use different retrieval and filter methods, they do not contain the same number of data (see Fig. 20). Currently, the NASA ACOS product has the largest number of valid data points, followed by the new GOSAT-FOCAL product with about 20% less data.

5.1 Direct comparisons

There are enough common measurement points included in the different GOSAT products to perform a direct comparison. 405 Figure 21 shows exemplary a comparison between the GOSAT-FOCAL data for the year 2018 with the corresponding ACOS, BESD, SRON, NIES and UoL products. For each plot we only use data where both data sets have a valid XCO₂ value. For these data we performed a linear regression using the Orthogonal Distance Regression (ODR) method (see e.g. Boggs et al., 1987). Unlike common linear regression, ODR considers uncertainties for both axes (data sets) by minimising the orthogonal distances between the model curve and the data points. The ODR results are shown by the red line and its label. Number of 410 collocations and median/mean and standard deviations of the differences are given in the titles.

Overall, the data scatter around the 1:1 line in a similar way for all comparisons. ODR slopes vary between the data sets from 0.84 (for FOCAL vs. ACOS) up to 1.08 (for FOCAL vs. BESD). Most collocations are available for the ACOS data set because this has the largest number of valid data. Mean and median differences are quite similar and reach from -0.17 ppm (comparison to BESD) to 0.67 ppm (comparison with UoL). The scatter (standard deviation of the differences) reaches from 415 1.4 ppm (ACOS, NIES) to 1.8 ppm (BESD).

5.2 TCCON comparisons

The TCCON network provides high-quality XCO₂ (and other) data which are currently considered to be the main reference for greenhouse gas data obtained from satellite measurements. Therefore we compared the different GOSAT data sets with collocated TCCON measurements from 2009 to the end of 2018. BESD data are not included, because they do not cover the 420 complete time interval. Collocation criteria are:

- Maximum time difference of 2 h.
- Maximum spatial distance of satellite measurement from TCCON station 500 km.
- Maximum surface elevation difference between satellite measurement and TCCON station 250 m.



In addition to these criteria we also consider in the validation only stations / TCCON data sets, which have at least 50
425 collocations for all algorithms. This improves the comparability of regional and seasonal biases. As a consequence, not all
stations listed in Tab. 1 contribute to the validation.

The comparison procedure is the same as used by Reuter et al. (2020) and described by Reuter et al. (version 3.1, 03-
11-2019). In summary, for each TCCON site, the time series of satellite minus TCCON differences are computed under
consideration of the averaging kernels, i.e. different vertical sensitivities. The resulting time series are fitted with a trend
430 model, which includes an offset term, a slope term, and a sine term for seasonal fluctuations. The offset term is considered the
station bias and the station scatter is computed from the standard deviation of the fit residual. Results for the time series at the
TCCON stations are shown in Fig. 22. Overall, the temporal variations of XCO₂ are well reproduced by all data.

Figure 23 shows as a summary of the TCCON comparisons the derived bias and scatter for the different stations and products.
The new GOSAT-FOCAL product compares well with the other data sets. Its differences to TCCON have a station to station
435 bias (the standard deviation of the station bias) of 0.56 ppm and a mean scatter (RMS scatter per station) of 1.89 ppm. The
seasonal component of the bias has a station to station average standard deviation of 0.37 ppm. Overall, the ACOS product
performs best in this comparison.

Note that the biases shown in Fig. 23 correspond essentially to a bias anomaly since a global bias was removed from all
products. Therefore different signs of biases for different products could be coincidental. However, the biases of FOCAL and
440 ACOS are consistent with the biases found by Reuter et al. (2020).

Via the TCCON comparison it is also possible to validate the reported precision of the FOCAL data products (i.e. the
specified XCO₂ error). The basic idea is to estimate the “true” precision from the variability of the XCO₂ bias relative to
trend-corrected, collocated TCCON data. For this purpose, we define 20 bins with increasing reported XCO₂ uncertainty and
compute the corresponding true precision from the scatter relative to TCCON (i.e., the fit residual mentioned above).

The corresponding scatter plot is shown in Fig. 24. We use the fitted linear curve to correct the reported uncertainty of the
445 GOSAT-FOCAL data. After the correction, all data scatter around the 1:1 line (dashed).

A similar correction will be performed for the GOSAT-2 FOCAL product as soon as sufficient data (GOSAT-2 as well as
TCCON) are available, which is currently not yet the case.

5.3 Time series

450 To investigate the temporal behaviour of the FOCAL XCO₂ data sets, we performed comparisons based on monthly data from
2009 to 2019, which were spatially gridded to 5° × 5° (examples are shown in Figs. 18 and 19). Similar data sets have been
generated for the SRON, UoL, ACOS and NIES GOSAT products. We also produced a corresponding gridded GOSAT-BESD
data set; since these are near-real-time (NRT) data only, there are no GOSAT BESD data before 2014 available (when the NRT
processing started). GOSAT-2 data start in February 2019.

455 We then selected for each combination of GOSAT-FOCAL XCO₂ and a correlative data set grid points where the standard
error of the mean is less than 1.6 ppm (as a basic quality filter, similar as done by Reuter et al., 2020). These data were then
averaged over different latitudinal ranges, namely:



- Global (90°S – 90°N)
- Northern hemisphere (25°N – 90°N)
- 460 – Tropics (25°S – 25°N)
- Southern hemisphere (25°S – 90°S)

Figure 25 shows the results of these comparisons. The left plots display time series of the different data sets, the right plots the difference between the GOSAT-FOCAL XCO_2 and the reference data. All data products reproduce the overall increase of XCO_2 with time as well as the seasonal variations. On average, FOCAL data are typically about 0.5 ppm higher than the other data sets (except for BESD). This is most likely related to the choice of the “true” XCO_2 for the bias correction. There are long-term changes in the order of 1 ppm over the complete time series, which differ for each data set. For example, the GOSAT-FOCAL data show in the tropics relative to SRON a higher value at the start of the time series, but both data sets agree at the end. On the other hand, the average difference to the UoL data in the northern hemisphere is negative during the first years, but increases to an almost constant small positive offset below about 0.5 ppm. There is not much difference in the temporal behaviour between the GOSAT-FOCAL and the ACOS and NIES time series. The seasonal shapes also differ slightly with amplitudes of about 0.5 ppm with somewhat larger differences in the southern hemisphere where seasonal variations are generally smaller.

Overall, the agreement within the GOSAT data sets is broadly consistent with the systematic regional and seasonal biases derived from the TCCON validation, especially considering that all gridded data sets are based on a different spatial and temporal sampling. Also, the FOCAL products for GOSAT and GOSAT-2 seem to agree quite well, but more GOSAT-2 data is needed to confirm this.

6 Conclusions

Based on the FOCAL retrieval method a new XCO_2 data set for GOSAT and a first XCO_2 data set for GOSAT-2 have been generated, making use of both measured polarisation directions. The GOSAT-FOCAL data set compares well with corresponding data from other currently available GOSAT retrieval algorithms, i.e. the RemoTec product from SRON, the UoL FP product, the NASA ACOS product, the NIES product and the BESD product from IUP. All data sets use different filtering and bias correction schemes and therefore comprise also a different number and sampling of data. The GOSAT-FOCAL product performs well in this context and has almost as many valid data as the ACOS product. Based on gridded data, differences in long-term variations of all data sets in the order of 1 ppm per decade are observed. Also, seasonal variations differ by about 0.5 ppm.

Comparisons with ground-based TCCON data reveal for the GOSAT-FOCAL product an overall station to station bias of 0.56 ppm and a mean scatter of 1.89 ppm. These values are comparable to and in some cases even better than those of the already existing GOSAT products of which some have less valid data.

The first GOSAT-2 results using the FOCAL method are also quite promising, but further investigations, longer time series and more correlative data sets are required for a quantitative assessment of the GOSAT-2-FOCAL data quality.



490 Overall, the FOCAL method has proven to be computationally fast and to produce XCO₂ results with similar accuracy as other, typically more time consuming, retrieval algorithms. This is the case not only when applied to OCO-2 but also for GOSAT and GOSAT-2. FOCAL is therefore considered to be a good candidate algorithm for future satellite sensors producing large amounts of data, like the forthcoming European anthropogenic CO₂ Monitoring (CO2M) mission.

Data availability. The GOSAT-FOCAL V1.0 data set and the preliminary GOSAT-2-FOCAL data are available on request from the authors.

495 *Author contributions.* S. Noël adapted the FOCAL method to GOSAT and GOSAT-2, generated the FOCAL data products and performed the validation. M. Reuter developed the FOCAL method and provided the “true” databases and the TCCON validation tools. J. Borchardt provided the used python implementation for the SC4C methane climatology from O. Scheising. M. Hilker provided the original python implementation of FOCAL (OCO-2 version). A. Di Noia and Y. Yoshida provided the UoL and NIES GOSAT data products. H. Suto provided information on GOSAT and GOSAT-2, especially the preliminary GOSAT-2 ILS.

500 The following co-authors provided TCCON data: M. Buschmann, N. M. Deutscher, D. G. Feist, D. W. T. Griffith, F. Hase, R. Kivi, I. Morino, J. Notholt, H. Ohyama, C. Petri, J. R. Podolske, D. F. Pollard, M. K. Sha, K. Shiomi, R. Sussmann, Y. Té, V. A. Velasco, T. Warneke. All authors provided support in writing the paper.

Competing interests. The authors declare that they have no conflict of interest.

Acknowledgements. GOSAT and GOSAT-2 spectral data have been provided by JAXA and NIES. CarbonTracker CT2019 and CT-NRT.v2020-
505 1 results were provided by NOAA ESRL, Boulder, Colorado, USA from the website at <http://carbontracker.noaa.gov>. ABSCO cross sections for CO₂ were provided by NASA and the ACOS/OCO-2 team. GMTED2010 topography data were provided by the U.S. Geological Survey (USGS) and the National Geospatial-Intelligence Agency (NGA). We thank the European Center for Medium Range Weather Forecasts (ECMWF) for providing us with analysed meteorological fields (ERA5 data).

We thank the OCO-2 Science Team for the GOSAT ACOS Level 2 XCO₂ product obtained from https://oco2.gesdisc.eosdis.nasa.gov/data/GOSAT_TANSO_Level2/ACOS_L2_Lite_FP.9r/, <https://doi.org/10.5067/VWSABTO7ZII4>, last access: 16 October 2020. The SRON GOSAT XCO₂ data product has been obtained from the Copernicus Climate Data Store (<https://cds.climate.copernicus.eu/>, last access: 15-Oct-2020).

We used TCCON GGG2014 ground-based validation data (see Tab. 1). TCCON data from the Eureka and Izaña stations were provided by K. Strong and O. Garcia, respectively. The Ascension Island TCCON station has been supported by the European Space Agency (ESA)
515 under grant 4000120088/17/I-EF and by the German Bundesministerium für Wirtschaft und Energie (BMWi) under grants 50EE1711C and 50EE1711E. We thank the ESA Ariane Tracking Station at North East Bay, Ascension Island, for hosting and local support. The TCCON site at Réunion Island is operated by the Royal Belgian Institute for Space Aeronomy with financial support since 2014 by the EU project ICOS-Inwire and the ministerial decree for ICOS (FR/35/IC1 to FR/35/C5) and local activities supported by LACy/UMR8105 – Université



520 de La Réunion. The Paris TCCON site has received funding from Sorbonne Université, the French research center CNRS, the French space
agency CNES, and Région Île-de-France. The TCCON stations at Rikubetsu, Tsukuba and Burgos are supported in part by the GOSAT series
project. Local support for Burgos is provided by the Energy Development Corporation (EDC, Philippines). N. M. Deutscher is funded by
ARC Future Fellowship FT180100327. Darwin and Wollongong TCCON stations are supported by ARC grants DP160100598, LE0668470,
DP140101552, DP110103118 and DP0879468, and Darwin receives additional support from NASA grants NAG5-12247 and NNG05-
525 GD07G and technical assistance from the Australian Bureau of Meteorology. The TCCON stations Garmisch and Zugspitze have been
supported by the European Space Agency (ESA) under grant 4000120088/17/I-EF and by the German Bundesministerium für Wirtschaft
und Energie (BMWi) via the DLR under grant 50EE1711D as well as by the Helmholtz Society via the research program ATMO.

This work has received funding from JAXA (GOSAT and GOSAT-2 support, contracts 19RT000692 and JX-PSPC-527269), EUMETSAT
(FOCAL-CO2M study, contract EUM/CO/19/4600002372/RL), ESA (GHG-CCI+ project, contract 4000126450/19/I-NB) and the State and
the University of Bremen.



530 References

- Anderson, G., Clough, S., Kneizys, F., Chetwynd, J., and Shettle, E.: AFGL Atmospheric Constituent Profiles (0–120km), Environmental Research Papers No. 954, AFGL-TR-86-0110, https://www.researchgate.net/publication/235054307_AFGL_Atmospheric_Constituent_Profiles_0120km, 1986.
- Basu, S., Guerlet, S., Butz, A., Houweling, S., Hasekamp, O., Aben, I., Krummel, P., Steele, P., Langenfelds, R., Torn, M., Biraud, S.,
535 Stephens, B., Andrews, A., and Worthy, D.: Global CO₂ fluxes estimated from GOSAT retrievals of total column CO₂, *Atmos. Chem. Phys.*, 13, 8695–8717, <https://doi.org/10.5194/acp-13-8695-2013>, <http://www.atmos-chem-phys.net/13/8695/2013/>, 2013.
- Benner, D. C., Devi, V. M., Sung, K., Brown, L. R., Miller, C. E., Payne, V. H., Drouin, B. J., Yu, S., Crawford, T. J., Mantz, A. W.,
Smith, M. A. H., and Gamache, R. R.: Line parameters including temperature dependences of air- and self-broadened line shapes of
¹²C¹⁶O₂: 2.06- μ m region, *J. Mol. Spectr.*, 326, 21–47, <https://doi.org/https://doi.org/10.1016/j.jms.2016.02.012>, <http://www.sciencedirect.com/science/article/pii/S0022285216300261>, new Visions of Spectroscopic Databases, Volume I, 2016.
540
- Blumenstock, T., Hase, F., Schneider, M., García, O. E., and Sepúlveda, E.: TCCON data from Izana (ES), Release GGG2014.R1, <https://doi.org/10.14291/TCCON.GGG2014.IZANA01.R1>, <https://data.caltech.edu/records/302>, 2017.
- Boggs, P. T., Byrd, R. H., and Schnabel, R. B.: A Stable and Efficient Algorithm for Nonlinear Orthogonal Distance Regression, *SIAM J. Sci. Stat. Comput.*, 8, 1052–1078, <https://doi.org/10.1137/0908085>, <https://doi.org/10.1137/0908085>, 1987.
- 545 Bovensmann, H., Burrows, J. P., Buchwitz, M., Frerick, J., Noël, S., Rozanov, V. V., Chance, K. V., and Goede, A. H. P.: SCIAMACHY — Mission Objectives and Measurement Modes, *J. Atmos. Sci.*, 56, 127–150, 1999.
- Buchwitz, M., Reuter, M., Schneising, O., Noël, S., Gier, B., Bovensmann, H., Burrows, J. P., Boesch, H., Anand, J., Parker, R. J., Somkuti, P., Detmers, R. G., Hasekamp, O. P., Aben, I., Butz, A., Kuze, A., Suto, H., Yoshida, Y., Crisp, D., and O’Dell, C.: Computation and analysis of atmospheric carbon dioxide annual mean growth rates from satellite observations during 2003–2016, *Atmos. Chem. Phys.*, 18,
550 17 355–17 370, <https://doi.org/10.5194/acp-18-17355-2018>, <https://www.atmos-chem-phys.net/18/17355/2018/>, 2018.
- Burrows, J., Hölzle, E., Goede, A., Visser, H., and Fricke, W.: SCIAMACHY – scanning imaging absorption spectrometer for atmospheric cartography, *Acta Astr.*, 35, 445–451, [https://doi.org/https://doi.org/10.1016/0094-5765\(94\)00278-T](https://doi.org/https://doi.org/10.1016/0094-5765(94)00278-T), <http://www.sciencedirect.com/science/article/pii/009457659400278T>, earth Observation, 1995.
- Butz, A., Guerlet, S., Hasekamp, O., Schepers, D., Galli, A., Aben, I., Frankenberg, C., Hartmann, J.-M., Tran, H., Kuze, A., Keppel-
555 Aleks, G., Toon, G., Wunch, D., Wennberg, P., Deutscher, N., Griffith, D., Macatangay, R., Messerschmidt, J., Notholt, J., and Warneke, T.: Toward accurate CO₂ and CH₄ observations from GOSAT, *Geophys. Res. Lett.*, 38, <https://doi.org/10.1029/2011GL047888>, <https://agupubs.onlinelibrary.wiley.com/doi/abs/10.1029/2011GL047888>, 2011.
- Chevallier, F.: On the statistical optimality of CO₂ atmospheric inversions assimilating CO₂ column retrievals, *Atmos. Chem. Phys.*, pp. 11 133–11 145, <https://doi.org/10.5194/acp-15-11133-2015>, <https://www.atmos-chem-phys.net/15/11133/2015/>, 2015.
- 560 Chevallier, F., Palmer, P. I., Feng, L., Boesch, H., O’Dell, C. W., and Bousquet, P.: Towards robust and consistent regional CO₂ flux estimates from in situ and space-borne measurements of atmospheric CO₂, *Geophys. Res. Lett.*, 41, 1065–1070, <https://doi.org/10.1002/2013GL058772>, <http://dx.doi.org/10.1002/2013GL058772>, 2014.
- Ciais, P., Dolman, A. J., Bombelli, A., Duren, R., Peregón, A., Rayner, P. J., Miller, C., Gobron, N., Kinderman, G., Marland, G., Gruber, N., Chevallier, F., Andres, R. J., Balsamo, G., Bopp, L., Bréon, F.-M., Broquet, G., Dargaville, R., Battin, T. J., Borges, A., Bovensmann, H.,
565 Buchwitz, M., Butler, J., Canadell, J. G., Cook, R. B., DeFries, R., Engelen, R., Gurney, K. R., Heinze, C., Heimann, M., Held, A., Henry, M., Law, B., Luysaert, S., Miller, J., Moriyama, T., Moulin, C., Myneni, R. B., Nussli, C., Obersteiner, M., Ojima, D., Pan, Y., Paris, J.-D.,



- Piao, S. L., Poulter, B., Plummer, S., Quegan, S., Raymond, P., Reichstein, M., Rivier, L., Sabine, C., Schimel, D., Tarasova, O., Valentini, R., Wang, R., van der Werf, G., Wickland, D., Williams, M., and Zehner, C.: Current systematic carbon-cycle observations and the need for implementing a policy-relevant carbon observing system, *Biogeosciences*, 11, 3547–3602, <https://doi.org/10.5194/bg-11-3547-2014>, <http://www.biogeosciences.net/11/3547/2014/>, 2014.
- 570 Cogan, A. J., Boesch, H., Parker, R. J., Feng, L., Palmer, P. I., Blavier, J.-F. L., Deutscher, N. M., Macatangay, R., Notholt, J., Roehl, C., Warneke, T., and Wunch, D.: Atmospheric carbon dioxide retrieved from the Greenhouse gases Observing SATellite (GOSAT): Comparison with ground-based TCCON observations and GEOS-Chem model calculations, *Journal of Geophysical Research: Atmospheres*, 117, <https://doi.org/10.1029/2012JD018087>, <https://agupubs.onlinelibrary.wiley.com/doi/abs/10.1029/2012JD018087>, 2012.
- 575 Crisp, D., Atlas, R. M., Bréon, F.-M., Brown, L. R., Burrows, J. P., Ciaia, P., Connor, B. J., Doney, S. C., Fung, I. Y., Jacob, D. J., Miller, C. E., O'Brien, D., Pawson, S., Randerson, J. T., Rayner, P., Salawitch, R. S., Sander, S. P., Sen, B., Stephens, G. L., Tans, P. P., Toon, G. C., Wennberg, P. O., Wofsy, S. C., Yung, Y. L., Kuang, Z., Chudasama, B., Sprague, G., Weiss, P., Pollock, R., Kenyon, D., and Schroll, S.: The Orbiting Carbon Observatory (OCO) mission, *Adv. Space Res.*, 34, 700–709, 2004.
- Crisp, D., Pollock, H. R., Rosenberg, R., Chapsky, L., Lee, R. A. M., Oyafuso, F. A., Frankenberg, C., O'Dell, C. W., Bruegge, C. J., Doran, G. B., Eldering, A., Fisher, B. M., Fu, D., Gunson, M. R., Mandrake, L., Osterman, G. B., Schwandner, F. M., Sun, K., Taylor, T. E., Wennberg, P. O., and Wunch, D.: The on-orbit performance of the Orbiting Carbon Observatory-2 (OCO-2) instrument and its radiometrically calibrated products, *Atmos. Meas. Tech.*, 10, 59–81, <https://doi.org/10.5194/amt-10-59-2017>, <https://www.atmos-meas-tech.net/10/59/2017/>, 2017.
- 580 Danielson, J. and Gesch, D.: Global multi-resolution terrain elevation data 2010 (GMTED2010): Open-File Report 2011–1073, Tech. rep., U.S. Geological Survey, <https://doi.org/10.3133/ofr20111073>, <http://pubs.er.usgs.gov/publication/ofr20111073>, 2011.
- Davis, S. P., Abrams, M. C., and Brault, J. W.: 5 - Nonideal (real-world) interferograms, in: *Fourier Transform Spectrometry*, edited by Davis, S. P., Abrams, M. C., and Brault, J. W., pp. 67–80, Academic Press, San Diego, <https://doi.org/https://doi.org/10.1016/B978-012042510-5/50005-6>, <http://www.sciencedirect.com/science/article/pii/B9780120425105500056>, 2001.
- De Mazière, M., Sha, M. K., Desmet, F., Hermans, C., Scolas, F., Kumps, N., Metzger, J.-M., Dufлот, V., and Cammas, J.-P.: TCCON data from Réunion Island (RE), Release GGG2014.R1, <https://doi.org/10.14291/TCCON.GGG2014.REUNION01.R1>, <https://data.caltech.edu/records/322>, 2017.
- 590 Deutscher, N. M., Notholt, J., Messerschmidt, J., Weinzierl, C., Warneke, T., Petri, C., and Grupe, P.: TCCON data from Bialystok (PL), Release GGG2014.R2, <https://doi.org/10.14291/TCCON.GGG2014.BIALYSTOK01.R2>, <https://data.caltech.edu/records/1300>, 2019.
- Devi, V. M., Benner, D. C., Sung, K., Brown, L. R., Crawford, T. J., Miller, C. E., Drouin, B. J., Payne, V. H., Yu, S., Smith, M. A. H., Mantz, A. W., and Gamache, R. R.: Line parameters including temperature dependences of self- and air-broadened line shapes of $^{12}\text{C}^{16}\text{O}_2$: 1.6- μm region, *J. Quant. Spectr. Rad. Transf.*, 177, 117–144, <https://doi.org/https://doi.org/10.1016/j.jqsrt.2015.12.020>, <http://www.sciencedirect.com/science/article/pii/S0022407315301916>, XVIIIth Symposium on High Resolution Molecular Spectroscopy (HighRus-2015), Tomsk, Russia, 2016.
- Dubey, M., Lindenmaier, R., Henderson, B., Green, D., Allen, N., Roehl, C., Blavier, J.-F., Butterfield, Z., Love, S., Hamelmann, J., and Wunch, D.: TCCON data from Four Corners (US), Release GGG2014R0, TCCON data archive, hosted by CaltechDATA, <https://doi.org/10.14291/tcon.ggg2014.fourcorners01.R0/1149272>, <https://tcondata.org>, 2014.
- 600 Eldering, A., Wennberg, P. O., Crisp, D., Schimel, D. S., Gunson, M. R., Chatterjee, A., Liu, J., Schwandner, F. M., Sun, Y., O'Dell, C. W., Frankenberg, C., Taylor, T., Fisher, B., Osterman, G. B., Wunch, D., Hakkarainen, J., Tamminen, J., and Weir, B.: The Orbiting Carbon



- 605 Observatory-2 early science investigations of regional carbon dioxide fluxes, *Science*, 358, <https://doi.org/10.1126/science.aam5745>, <https://science.sciencemag.org/content/358/6360/eaam5745>, 2017.
- Eldering, A., Taylor, T. E., O'Dell, C. W., and Pavlick, R.: The OCO-3 mission: measurement objectives and expected performance based on 1 year of simulated data, *Atmos. Meas. Tech.*, 12, 2341–2370, <https://doi.org/10.5194/amt-12-2341-2019>, <https://www.atmos-meas-tech.net/12/2341/2019/>, 2019.
- Feist, D. G., Arnold, S. G., John, N., and Geibel, M. C.: TCCON data from Ascension Island (SH), Release GGG2014R0, TCCON data archive, hosted by CaltechDATA, <https://doi.org/10.14291/tcon.ggg2014.ascension01.R0/1149285>, <https://tcondata.org>, 2014.
- 610 Fletcher, R.: A Modified Marquardt Subroutine for Non-Linear Least Squares., Tech. Rep. AERE-R 6799, Atomic Energy Research Establishment, Harwell, UK, <https://ntrl.ntis.gov/NTRL/dashboard/searchResults/titleDetail/AERER6799.xhtml>, 1971.
- Friedlingstein, P., Jones, M. W., O'Sullivan, M., Andrew, R. M., Hauck, J., Peters, G. P., Peters, W., Pongratz, J., Sitch, S., Le Quéré, C., Bakker, D. C. E., Canadell, J. G., Ciais, P., Jackson, R. B., Anthoni, P., Barbero, L., Bastos, A., Bastrikov, V., Becker, M., Bopp, L., Buitenhuis, E., Chandra, N., Chevallier, F., Chini, L. P., Currie, K. I., Feely, R. A., Gehlen, M., Gilfillan, D., Gkritzalis, T., Goll, D. S., Gruber, N., Gutekunst, S., Harris, I., Haverd, V., Houghton, R. A., Hurtt, G., Ilyina, T., Jain, A. K., Joetzjer, E., Kaplan, J. O., Kato, E., Klein Goldewijk, K., Korsbakken, J. I., Landschützer, P., Lauvset, S. K., Lefèvre, N., Lenton, A., Lienert, S., Lombardozi, D., Marland, G., McGuire, P. C., Melton, J. R., Metzl, N., Munro, D. R., Nabel, J. E. M. S., Nakaoka, S.-I., Neill, C., Omar, A. M., Ono, T., Pregon, A., Pierrot, D., Poulter, B., Rehder, G., Resplandy, L., Robertson, E., Rödenbeck, C., Séférian, R., Schwinger, J., Smith, N., Tans, P. P., Tian, H., Tilbrook, B., Tubiello, F. N., van der Werf, G. R., Wiltshire, A. J., and Zaehle, S.: Global Carbon Budget 2019, *Earth System Science Data*, 11, 1783–1838, <https://doi.org/10.5194/essd-11-1783-2019>, <https://essd.copernicus.org/articles/11/1783/2019/>, 2019.
- 620 Gordon, I., Rothman, L., Hill, C., Kochanov, R., Tan, Y., Bernath, P., Birk, M., Boudon, V., Campargue, A., Chance, K., Drouin, B., Flaud, J.-M., Gamache, R., Hodges, J., Jacquemart, D., Perevalov, V., Perrin, A., Shine, K., Smith, M.-A., Tennyson, J., Toon, G., Tran, H., Tyuterev, V., Barbe, A., Császár, A., Devi, V., Furtenbacher, T., Harrison, J., Hartmann, J.-M., Jolly, A., Johnson, T., Karman, T., Kleiner, I., Kyuberis, A., Loos, J., Lyulin, O., Massie, S., Mikhailenko, S., Moazzen-Ahmadi, N., Müller, H., Naumenko, O., Nikitin, A., Polyansky, O., Rey, M., Rotger, M., Sharpe, S., Sung, K., Starikova, E., Tashkun, S., Auwera, J. V., Wagner, G., Wilzewski, J., Wcisło, P., Yu, S., and Zak, E.: The HITRAN2016 molecular spectroscopic database, *J. Quant. Spectr. Rad. Transf.*, 203, 3 – 69, <https://doi.org/https://doi.org/10.1016/j.jqsrt.2017.06.038>, <http://www.sciencedirect.com/science/article/pii/S0022407317301073>, HITRAN2016 Special Issue, 2017.
- 630 Gottwald, M. and Bovensmann, H., eds.: *SCIAMACHY - Exploring the Changing Earth's Atmosphere*, Springer Dordrecht Heidelberg London New York, <https://doi.org/10.1007/978-90-481-9896-2>, 2011.
- Griffith, D. W., Deutscher, N. M., Velazco, V. A., Wennberg, P. O., Yavin, Y., Aleks, G. K., Washenfelder, R. a., Toon, G. C., Blavier, J.-F., Murphy, C., Jones, N., Kettlewell, G., Connor, B. J., Macatangay, R., Roehl, C., Ryzcek, M., Glowacki, J., Culligan, T., and Bryant, G.: TCCON data from Darwin (AU), Release GGG2014R0, TCCON data archive, hosted by CaltechDATA, <https://doi.org/10.14291/tcon.ggg2014.darwin01.R0/1149290>, <https://tcondata.org>, 2014a.
- 635 Griffith, D. W., Velazco, V. A., Deutscher, N. M., Murphy, C., Jones, N., Wilson, S., Macatangay, R., Kettlewell, G., Buchholz, R. R., and Riggensbach, M.: TCCON data from Wollongong (AU), Release GGG2014R0, TCCON data archive, hosted by CaltechDATA, <https://doi.org/10.14291/tcon.ggg2014.wollongong01.R0/1149291>, <https://tcondata.org>, 2014b.
- Hase, F., Blumenstock, T., Dohe, S., Gross, J., and Kiel, M.: TCCON data from Karlsruhe (DE), Release GGG2014R1, TCCON data archive, hosted by CaltechDATA, <https://doi.org/10.14291/tcon.ggg2014.karlsruhe01.R1/1182416>, <https://tcondata.org>, 2014.
- 640



- Hersbach, H., Bell, B., Berrisford, P., Hirahara, S., Horányi, A., Muñoz Sabater, J., Nicolas, J., Peubey, C., Radu, R., Schepers, D., Simmons, A., Soci, C., Abdalla, S., Abellan, X., Balsamo, G., Bechtold, P., Biavati, G., Bidlot, J., Bonavita, M., De Chiara, G., Dahlgren, P., Dee, D., Diamantakis, M., Dragani, R., Flemming, J., Forbes, R., Fuentes, M., Geer, A., Haimberger, L., Healy, S., Hogan, R. J., Hólm, E., Janisková, M., Keeley, S., Laloyaux, P., Lopez, P., Lupu, C., Radnoti, G., de Rosnay, P., Rozum, I., Vamborg, F., Villaume, S., and Thépaut, J.-N.: The ERA5 global reanalysis, *Quart. Jour. R. Met. Soc.*, pp. 1–51, <https://doi.org/10.1002/qj.3803>, <https://rmets.onlinelibrary.wiley.com/doi/abs/10.1002/qj.3803>, 2020.
- 645 Heymann, J., Reuter, M., Hilker, M., Buchwitz, M., Schneising, O., Bovensmann, H., Burrows, J. P., Kuze, A., Suto, H., Deutscher, N. M., Dubey, M. K., Griffith, D. W. T., Hase, F., Kawakami, S., Kivi, R., Morino, I., Petri, C., Roehl, C., Schneider, M., Sherlock, V., Sussmann, R., Velazco, V. A., Warneke, T., and Wunch, D.: Consistent satellite XCO₂ retrievals from SCIAMACHY and GOSAT using the BESD
650 algorithm, *Atmos. Meas. Tech.*, 8, 2961–2980, <https://doi.org/10.5194/amt-8-2961-2015>, <https://www.atmos-meas-tech.net/8/2961/2015/>, 2015.
- Houweling, S., Baker, D., Basu, S., Boesch, H., Butz, A., Chevallier, F., Deng, F., Dlugokencky, E. J., Feng, L., Ganshin, A., and et al.: An inter-comparison of inverse models for estimating sources and sinks of CO₂ using GOSAT measurements, *J. Geophys. Res.*, <https://doi.org/10.1002/2014jd022962>, <http://dx.doi.org/10.1002/2014JD022962>, 2015.
- 655 IPCC: Climate Change 2013: The Physical Science Basis. Contribution of Working Group I to the Fifth Assessment Report of the Intergovernmental Panel on Climate Change, Cambridge University Press, Cambridge, United Kingdom and New York, NY, USA, 2013.
- Iraci, L. T., Podolske, J., Hillyard, P. W., Roehl, C., Wennberg, P. O., Blavier, J.-F., Allen, N., Wunch, D., Osterman, G. B., and Albertson, R.: TCCON data from Edwards (US), Release GGG2014R1, TCCON data archive, hosted by CaltechDATA, <https://doi.org/10.14291/tcon.ggg2014.edwards01.R1/1255068>, <https://tcondata.org>, 2016a.
- 660 Iraci, L. T., Podolske, J., Hillyard, P. W., Roehl, C., Wennberg, P. O., Blavier, J.-F., Landeros, J., Allen, N., Wunch, D., Zavaleta, J., Quigley, E., Osterman, G. B., Barrow, E., and Barney, J.: TCCON data from Indianapolis (US), Release GGG2014R1, TCCON data archive, hosted by CaltechDATA, <https://doi.org/10.14291/tcon.ggg2014.indianapolis01.R1/1330094>, <https://tcondata.org>, 2016b.
- Jacobson, A. R., Schuldt, K. N., Miller, J. B., Oda, T., Tans, P., Arlyn Andrews, Mund, J., Ott, L., Collatz, G. J., Aalto, T., Afshar, S., Aikin, K., Aoki, S., Apadula, F., Baier, B., Bergamaschi, P., Beyersdorf, A., Biraud, S. C., Bollenbacher, A., Bowling, D., Brailsford, G., Abshire, J. B., Chen, G., Huilin Chen, Lukasz Chmura, Sites Climadat, Colomb, A., Conil, S., Cox, A., Cristofanelli, P., Cuevas, E., Curcoll, R., Sloop, C. D., Davis, K., Wekker, S. D., Delmotte, M., DiGangi, J. P., Dlugokencky, E., Ehleringer, J., Elkins, J. W., Emmenegger, L., Fischer, M. L., Forster, G., Frumau, A., Galkowski, M., Gatti, L. V., Gloor, E., Griffis, T., Hammer, S., Haszpra, L., Hatakka, J., Heliasz, M., Hensen, A., Hermanssen, O., Hintsa, E., Holst, J., Jaffe, D., Karion, A., Kawa, S. R., Keeling, R., Keronen, P., Kolari, P., Kominkova, K., Kort, E., Krummel, P., Kubistin, D., Labuschagne, C., Langenfelds, R., Laurent, O., Laurila, T., Lauvaux, T., Law, B., Lee, J., Lehner, I., Leuenberger, M., Levin, I., Levula, J., Lin, J., Lindauer, M., Loh, Z., Lopez, M., Myhre, C. L., Machida, T., Mammarella, I., Manca, G., Manning, A., Manning, A., Marek, M. V., Marklund, P., Martin, M. Y., Matsueda, H., McKain, K., Meijer, H., Meinhardt, F., Miles, N., Miller, C. E., Mölder, M., Montzka, S., Moore, F., Josep-Anton Morgui, Morimoto, S., Munger, B., Jaroslaw Necki, Newman, S., Nichol, S., Niwa, Y., O’Doherty, S., Mikael Ottosson-Löfvenius, Paplawsky, B., Peischl, J., Peltola, O., Jean-Marc Pichon, Piper, S., Plass-Dölmer, C., Ramonet, M., Reyes-Sanchez, E., Richardson, S., Riris, H., Ryerson, T., Saito, K., Sargent, M., Sasakawa, M., Sawa, Y., Say, D., Scheeren, B., Schmidt, M., Schmidt, A., Schumacher, M., Shepson, P., Shook, M., Stanley, K., Steinbacher, M., Stephens, B., Sweeney, C., Thoning, K., Torn, M., Turnbull, J., Tørseth, K., Bulk, P. V. D., Laan-Luijkx, I. T. V. D., Dinther, D. V., Vermeulen, A., Viner, B., Vitkova, G., Walker, S., Weyrauch, D., Wofsy, S., Worthy, D., Dickon Young, and Miroslaw Zimnoch: CarbonTracker CT2019, <https://doi.org/10.25925/39M3-6069>, <https://www.esrl.noaa.gov/gmd/ccgg/carbontracker/CT2019/>, 2020a.
- 670



- Jacobson, A. R., Schuldt, K. N., Miller, J. B., Tans, P., Arlyn Andrews, Mund, J., Aalto, T., Bakwin, P., Bergamaschi, P., Biraud, S. C.,
680 Huilin Chen, Colomb, A., Conil, S., Cristofanelli, P., Davis, K., Delmotte, M., DiGangi, J. P., Dlugokencky, E., Emmenegger, L., Fischer,
M. L., Hatakka, J., Heliassz, M., Hermanssen, O., Holst, J., Jaffe, D., Karion, A., Keronen, P., Kominkova, K., Kubistin, D., Laurent, O.,
Laurila, T., Lee, J., Lehner, I., Leuenberger, M., Lindauer, M., Mikael Ottosson Löfvenius, Lopez, M., Mammarella, I., Manca, G., Marek,
M. V., Marklund, P., Martin, M. Y., McKain, K., Miller, C. E., Mölder, M., Myhre, C. L., Pichon, J. M., Plass-Dölmer, C., Ramonet, M.,
Scheeren, B., Schumacher, M., Sloop, C. D., Steinbacher, M., Sweeney, C., Thoning, K., Tørseth, K., Turnbull, J., Viner, B., Vitkova, G.,
685 Wekker, S. D., Weyrauch, D., and Worthy, D.: CarbonTracker Near Real-Time, CT-NRT.v2020-1, <https://doi.org/10.25925/RCHH-MS75>,
<https://www.esrl.noaa.gov/gmd/ccgg/carbontracker/CT-NRT.v2020-1/>, 2020b.
- Janssens-Maenhout, G., Pinty, B., Dowell, M., Zunker, H., Andersson, E., Balsamo, G., Bézy, J.-L., Brunhes, T., Bäsch, H., Bojkov, B.,
Brunner, D., Buchwitz, M., Crisp, D., Ciais, P., Counet, P., Dee, D., Denier van der Gon, H., Dolman, H., Drinkwater, M., Dubovik, O.,
Engelen, R., Fehr, T., Fernandez, V., Heimann, M., Holmlund, K., Houweling, S., Husband, R., Juvyns, O., Kentarchos, A., Landgraf, J.,
690 Lang, R., Löscher, A., Marshall, J., Meijer, Y., Nakajima, M., Palmer, P., Peylin, P., Rayner, P., Scholze, M., Sierk, B., Tamminen, J., and
Veefkind, P.: Towards an operational anthropogenic CO₂ emissions monitoring and verification support capacity, *Bull. Am. Met. Soc.*,
<https://doi.org/10.1175/BAMS-D-19-0017.1>, <https://doi.org/10.1175/BAMS-D-19-0017.1>, 2020.
- Kaminski, T., Scholze, M., Vossbeck, M., Knorr, W., Buchwitz, M., and Reuter, M.: Constraining a terrestrial biosphere model with remotely
sensed atmospheric carbon dioxide, *Rem. Sens. Env.*, <https://doi.org/10.1016/j.rse.2017.08.017>, <http://www.sciencedirect.com/science/article/pii/S0034425717303838>, 2017.
- 695 Kawakami, S., Ohshima, H., Arai, K., Okumura, H., Taura, C., Fukamachi, T., and Sakashita, M.: TCCON data from Saga (JP), Re-
lease GGG2014R0, TCCON data archive, hosted by CaltechDATA, <https://doi.org/10.14291/tcon.ggg2014.saga01.R0/1149283>, <https://tcondata.org>, 2014.
- Kiel, M., O'Dell, C. W., Fisher, B., Eldering, A., Nassar, R., MacDonald, C. G., and Wennberg, P. O.: How bias correction goes wrong:
700 measurement of XCO₂ affected by erroneous surface pressure estimates, *Atmos. Meas. Tech.*, 12, 2241–2259, <https://doi.org/10.5194/amt-12-2241-2019>, <https://www.atmos-meas-tech.net/12/2241/2019/>, 2019.
- Kikuchi, N., Yoshida, Y., Uchino, O., Morino, I., and Yokota, T.: An advanced retrieval algorithm for greenhouse gases using polar-
ization information measured by GOSAT TANSO-FTS SWIR I: Simulation study, *J. Geophys. Res. Atmos.*, 121, 13,129–13,157,
<https://doi.org/10.1002/2015JD024720>, <https://agupubs.onlinelibrary.wiley.com/doi/abs/10.1002/2015JD024720>, 2016.
- 705 Kivi, R., Heikkinen, P., and Kyrö, E.: TCCON data from Sodankyla (FI), Release GGG2014R0, TCCON data archive, hosted by Caltech-
DATA, <https://doi.org/10.14291/tcon.ggg2014.sodankyla01.R0/1149280>, <https://tcondata.org>, 2014.
- Kuhlmann, G., Broquet, G., Marshall, J., Clément, V., Löscher, A., Meijer, Y., and Brunner, D.: Detectability of CO₂ emission plumes of
cities and power plants with the Copernicus Anthropogenic CO₂ Monitoring (CO2M) mission, *Atmos. Meas. Tech.*, 12, 6695–6719,
<https://doi.org/10.5194/amt-12-6695-2019>, <https://amt.copernicus.org/articles/12/6695/2019/>, 2019.
- 710 Kuze, A., Suto, H., Nakajima, M., and Hamazaki, T.: Thermal and near infrared sensor for carbon observation Fourier-transform
spectrometer on the Greenhouse Gases Observing Satellite for greenhouse gases monitoring, *Appl. Optics*, 48, 6716–6733,
<https://doi.org/10.1364/AO.48.006716>, <http://ao.osa.org/abstract.cfm?URI=ao-48-35-6716>, 2009.
- Kuze, A., Suto, H., Shiomi, K., Kawakami, S., Tanaka, M., Ueda, Y., Deguchi, A., Yoshida, J., Yamamoto, Y., Kataoka, F., Taylor, T. E., and
Buijs, H. L.: Update on GOSAT TANSO-FTS performance, operations, and data products after more than 6 years in space, *Atmos. Meas.*
715 *Tech.*, 9, 2445–2461, <https://doi.org/10.5194/amt-9-2445-2016>, <https://amt.copernicus.org/articles/9/2445/2016/>, 2016.



- Kuze, A., Kikuchi, N., Kataoka, F., Suto, H., Shiomi, K., and Kondo, Y.: Detection of Methane Emission from a Local Source Using GOSAT Target Observations, *Rem. Sens.*, 12, <https://doi.org/10.3390/rs12020267>, <https://www.mdpi.com/2072-4292/12/2/267>, 2020.
- Labzovskii, L. D., Jeong, S.-J., and Parazoo, N. C.: Working towards confident spaceborne monitoring of carbon emissions from cities using Orbiting Carbon Observatory-2, *Rem. Sens. Env.*, 233, 111 359, <https://doi.org/https://doi.org/10.1016/j.rse.2019.111359>, <http://www.sciencedirect.com/science/article/pii/S0034425719303785>, 2019.
- 720 Liu, C., Wang, W., Sun, Y., and , : TCCON data from Hefei (PRC), Release GGG2014.R0, <https://doi.org/10.14291/TCCON.GGG2014.HEFEI01.R0>, <https://data.caltech.edu/records/1092>, 2018.
- Liu, J., Bowman, K. W., Schimel, D. S., Parazoo, N. C., Jiang, Z., Lee, M., Bloom, A. A., Wunch, D., Frankenberg, C., Sun, Y., O'Dell, C. W., Gurney, K. R., Menemenlis, D., Gierach, M., Crisp, D., and Eldering, A.: Contrasting carbon cycle responses of the tropical
725 continents to the 2015–2016 El Niño, *Science*, 358, <https://doi.org/10.1126/science.aam5690>, <https://science.sciencemag.org/content/358/6360/eaam5690>, 2017.
- Meftah, M., Damé, L., Bolsée, D., Hauchecorne, A., Pereira, N., Sluse, D., Cessateur, G., Irbah, A., Bureau, J., Weber, M., Bramstedt, K., Hilbig, T., Thiéblemont, R., Marchand, M., Lefèvre, F., Sarkissian, A., and Bekki, S.: SOLAR-ISS: A new reference spectrum based on SOLAR/SOLSPEC observations, *Astron. Astrophys.*, 611, A1, <https://doi.org/10.1051/0004-6361/201731316>, <https://doi.org/10.1051/0004-6361/201731316>, 2018.
- 730 Miller, S. M., Michalak, A. M., Detmers, R. G., Hasekamp, O. P., Bruhwiler, L. M. P., and Schwietzke, S.: China's coal mine methane regulations have not curbed growing emissions, *Nat. Commun.*, 10, <https://doi.org/10.1038/s41467-018-07891-7>, 2019.
- Morino, I., Yokozeki, N., Matzuzaki, T., and Horikawa, M.: TCCON data from Rikubetsu (JP), Release GGG2014R2, TCCON data archive, hosted by CaltechDATA, <https://doi.org/10.14291/tcon.ggg2014.rikubetsu01.R2>, <https://tcondata.org>, 2017.
- 735 Morino, I., Matsuzaki, T., and Horikawa, M.: TCCON data from Tsukuba (JP), 125HR, Release GGG2014.R2, <https://doi.org/10.14291/TCCON.GGG2014.TSUKUBA02.R2>, <https://data.caltech.edu/records/958>, 2018a.
- Morino, I., Velazco, V. A., Akihiro, H., Osamu, U., and Griffith, D. W. T.: TCCON data from Burgos, Ilocos Norte (PH), Release GGG2014.R0, TCCON data archive, hosted by CaltechDATA, <https://doi.org/10.14291/tcon.ggg2014.burgos01.R0>, <https://tcondata.org>, 2018b.
- 740 Nakajima, M., Suto, H., Yotsumoto, K., Shiomi, K., and Hirabayashi, T.: Fourier transform spectrometer on GOSAT and GOSAT-2, in: International Conference on Space Optics — ICSO 2014, edited by Sodnik, Z., Cugny, B., and Karafolas, N., vol. 10563, pp. 1354 – 1362, International Society for Optics and Photonics, SPIE, <https://doi.org/10.1117/12.2304062>, <https://doi.org/10.1117/12.2304062>, 2017.
- Nassar, R., Hill, T. G., McLinden, C. A., Wunch, D., Jones, D., and Crisp, D.: Quantifying CO₂ emissions from individual power plants from space, *Geophysical Research Letters*, 44, <https://doi.org/10.1002/2017GL074702>, 2017.
- 745 Notholt, J., Petri, C., Warneke, T., Deutscher, N. M., Palm, M., Buschmann, M., Weinzierl, C., Macatangay, R. C., and Grupe, P.: TCCON data from Bremen (DE), Release GGG2014.R1, <https://doi.org/10.14291/TCCON.GGG2014.BREMEN01.R1>, <https://data.caltech.edu/records/1290>, 2019a.
- Notholt, J., Schrems, O., Warneke, T., Deutscher, N., Weinzierl, C., Palm, M., Buschmann, M., and Engineers, A.-P. S.: TCCON data from Ny Ålesund, Spitsbergen (NO), Release GGG2014.R1, <https://doi.org/10.14291/tcon.ggg2014.nyalesund01.R1>, <https://doi.org/10.14291/tcon.ggg2014.nyalesund01.R1>, 2019b.
- 750 O'Dell, C. W., Connor, B., Bösch, H., O'Brien, D., Frankenberg, C., Castano, R., Christi, M., Eldering, D., Fisher, B., Gunson, M., McDuffie, J., Miller, C. E., Natraj, V., Oyafuso, F., Polonsky, I., Smyth, M., Taylor, T., Toon, G. C., Wennberg, P. O., and Wunch, D.:



- The ACOS CO₂ retrieval algorithm - Part 1: Description and validation against synthetic observations, *Atmos. Meas. Tech.*, 5, 99–121, <https://doi.org/10.5194/amt-5-99-2012>, <http://www.atmos-meas-tech.net/5/99/2012/>, 2012.
- 755 O'Dell, C. W., Eldering, A., Wennberg, P. O., Crisp, D., Gunson, M. R., Fisher, B., Frankenberg, C., Kiel, M., Lindqvist, H., Mandrake, L., Merrelli, A., Natraj, V., Nelson, R. R., Osterman, G. B., Payne, V. H., Taylor, T. E., Wunch, D., Drouin, B. J., Oyafuso, F., Chang, A., McDuffie, J., Smyth, M., Baker, D. F., Basu, S., Chevallier, F., Crowell, S. M. R., Feng, L., Palmer, P. I., Dubey, M., García, O. E., Griffith, D. W. T., Hase, F., Iraci, L. T., Kivi, R., Morino, I., Notholt, J., Ohyama, H., Petri, C., Roehl, C. M., Sha, M. K., Strong, K., Sussmann, R., Te, Y., Uchino, O., and Velazco, V. A.: Improved retrievals of carbon dioxide from Orbiting Carbon Observatory-2 with the version 8
760 ACOS algorithm, *Atmos. Meas. Tech.*, 11, 6539–6576, <https://doi.org/10.5194/amt-11-6539-2018>, <https://www.atmos-meas-tech.net/11/6539/2018/>, 2018.
- Palmer, P. I. and Feng, L., Baker, D., Chevallier, F., Bösch, H., and Somkuti, P.: Net carbon emissions from African biosphere dominate pan-tropical atmospheric CO₂ signal, *Nat. Commun.*, 10, 9, <https://www.nature.com/articles/s41467-019-11097-w>, 2019.
- Pedregosa, F., Varoquaux, G., Gramfort, A., Michel, V., Thirion, B., Grisel, O., Blondel, M., Prettenhofer, P., Weiss, R., Dubourg, V.,
765 Vanderplas, J., Passos, A., Cournapeau, D., Brucher, M., Perrot, M., and Édouard Duchesnay: Scikit-learn: Machine Learning in Python, *J. Machine Learning Res.*, 12, 2825–2830, <http://jmlr.org/papers/v12/pedregosa11a.html>, 2011.
- Pollard, D. F., Robinson, J., and Shiona, H.: TCCON data from Lauder (NZ), Release GGG2014.R0, <https://doi.org/10.14291/TCCON.GGG2014.LAUDER03.R0>, <https://data.caltech.edu/records/1220>, 2019.
- Rascher, U., Agati, G., Alonso, L., Cecchi, G., Champagne, S., Colombo, R., Damm, A., Daumard, F., de Miguel, E., Fernandez, G.,
770 Franch, B., Franke, J., Gerbig, C., Gioli, B., Gómez, J. A., Goulas, Y., Guanter, L., Gutiérrez-de-la Cámara, O., Hamdi, K., Hostert, P., Jiménez, M., Kosvancova, M., Lognoli, D., Meroni, M., Miglietta, F., Moersch, A., Moreno, J., Moya, I., Neininger, B., Okujeni, A., Ounis, A., Palombi, L., Raimondi, V., Schickling, A., Sobrino, J. A., Stellmes, M., Toci, G., Toscano, P., Udelhoven, T., van der Linden, S., and Zaldei, A.: CEFLES2: the remote sensing component to quantify photosynthetic efficiency from the leaf to the region by measuring sun-induced fluorescence in the oxygen absorption bands, *Biogeosciences*, 6, 1181–1198, <https://doi.org/10.5194/bg-6-1181-2009>, <https://www.biogeosciences.net/6/1181/2009/>, 2009.
- 775 Reuter, M., Buchwitz, M., Schneising, O., Heymann, J., Bovensmann, H., and Burrows, J. P.: A method for improved SCIAMACHY CO₂ retrieval in the presence of optically thin clouds, *Atmos. Meas. Tech.*, 3, 209–232, <https://doi.org/10.5194/amt-3-209-2010>, <http://dx.doi.org/10.5194/amt-3-209-2010>, 2010.
- Reuter, M., Bovensmann, H., Buchwitz, M., Burrows, J. P., Connor, B. J., Deutscher, N. M., Griffith, D. W. T., Heymann, J., Keppel-Aleks, G.,
780 Messerschmidt, J., Notholt, J., Petri, C., Robinson, J., Schneising, O., Sherlock, V., Velazco, V., Warneke, T., Wennberg, P. O., and Wunch, D.: Retrieval of atmospheric CO₂ with enhanced accuracy and precision from SCIAMACHY: Validation with FTS measurements and comparison with model results., *J. Geophys. Res.*, 116, <https://doi.org/10.1029/2010JD015047>, <http://dx.doi.org/10.1029/2010JD015047>, 2011.
- Reuter, M., Buchwitz, M., Schneising, O., Hase, F., Heymann, J., Guerlet, S., Cogan, A. J., Bovensmann, H., and Burrows, J. P.: A simple
785 empirical model estimating atmospheric CO₂ background concentrations, *Atmos. Meas. Tech.*, 5, 1349–1357, <https://doi.org/10.5194/amt-5-1349-2012>, <https://www.atmos-meas-tech.net/5/1349/2012/>, 2012.
- Reuter, M., Buchwitz, M., Hilboll, A., Richter, A., Schneising, O., Hilker, M., Heymann, J., Bovensmann, H., and Burrows, J.: Decreasing emissions of NO_x relative to CO₂ in East Asia inferred from satellite observations, *Nature Geosc.*, 7, 792, 2014a.
- Reuter, M., Buchwitz, M., Hilker, M., Heymann, J., Schneising, O., Pillai, D., Bovensmann, H., Burrows, J. P., Bösch, H., Parker, R., Butz,
790 A., Hasekamp, O., O'Dell, C. W., Yoshida, Y., Gerbig, C., Nehr Korn, T., Deutscher, N. M., Warneke, T., Notholt, J., Hase, F., Kivi, R.,



- Sussmann, R., Machida, T., Matsueda, H., and Sawa, Y.: Satellite-inferred European carbon sink larger than expected, *Atmos. Chem. Phys.*, 14, 13 739–13 753, <https://doi.org/10.5194/acp-14-13739-2014>, <http://www.atmos-chem-phys.net/14/13739/2014/>, 2014b.
- Reuter, M., Buchwitz, M., Hilker, M., Heymann, J., Bovensmann, H., Burrows, J. P., Houweling, S., Liu, Y. Y., Nassar, R., Chevallier, F., Ciais, P., Marshall, J., and Reichstein, M.: How Much CO₂ Is Taken Up by the European Terrestrial Biosphere?, *Bull. Am. Met. Soc.*, 98, 795 665–671, <https://doi.org/10.1175/BAMS-D-15-00310.1>, 2017a.
- Reuter, M., Buchwitz, M., Schneising, O., Noël, S., Bovensmann, H., and Burrows, J. P.: A Fast Atmospheric Trace Gas Retrieval for Hyperspectral Instruments Approximating Multiple Scattering – Part 2: Application to XCO₂ Retrievals from OCO-2, *Rem. Sens.*, 9, 1102, <https://doi.org/10.3390/rs9111102>, <http://www.mdpi.com/2072-4292/9/11/1102>, 2017b.
- Reuter, M., Buchwitz, M., Schneising, O., Noël, S., Rozanov, V., Bovensmann, H., and Burrows, J. P.: A Fast Atmospheric Trace Gas
800 Retrieval for Hyperspectral Instruments Approximating Multiple Scattering – Part 1: Radiative Transfer and a Potential OCO-2 XCO₂ Retrieval Setup, *Rem. Sens.*, 9, 1159, <https://doi.org/10.3390/rs9111159>, <http://www.mdpi.com/2072-4292/9/11/1159>, 2017c.
- Reuter, M., Buchwitz, M., Schneising, O., Krautwurst, S., O’Dell, C. W., Richter, A., Bovensmann, H., and Burrows, J. P.: Towards monitoring localized CO₂ emissions from space: co-located regional CO₂ and NO₂ enhancements observed by the OCO-2 and S5P satellites, *Atmos. Chem. Phys.*, 19, 9371–9383, <https://doi.org/10.5194/acp-19-9371-2019>, <https://www.atmos-chem-phys.net/19/9371/2019/>, 2019.
- 805 Reuter, M., Buchwitz, M., Schneising, O., Noël, S., Bovensmann, H., Burrows, J. P., Boesch, H., Di Noia, A., Anand, J., Parker, R. J., Somkuti, P., Wu, L., Hasekamp, O. P., Aben, I., Kuze, A., Suto, H., Shiomi, K., Yoshida, Y., Morino, I., Crisp, D., O’Dell, C. W., Notholt, J., Petri, C., Warneke, T., Velazco, V. A., Deutscher, N. M., Griffith, D. W. T., Kivi, R., Pollard, D. F., Hase, F., Sussmann, R., Té, Y. V., Strong, K., Roche, S., Sha, M. K., De Mazière, M., Feist, D. G., Iraci, L. T., Roehl, C. M., Retscher, C., and Schepers, D.: Ensemble-based satellite-derived carbon dioxide and methane column-averaged dry-air mole fraction data sets (2003–2018) for carbon and climate applications,
810 *Atmos. Meas. Tech.*, 13, 789–819, <https://doi.org/10.5194/amt-13-789-2020>, <https://www.atmos-meas-tech.net/13/789/2020/>, 2020.
- Reuter, M., Buchwitz, M., and Schneising-Weigel, O.: ProductQuality Assessment Report (PQAR) – ANNEX D for products XCO₂_EMMA, XCH₄_EMMA, XCO₂_OBS4MIPS, XCH₄_OBS4MIPS (v4.1, 2003–2018), Tech. rep., Copernicus Climate Change Service (C3S, http://www.iup.uni-bremen.de/carbon_ghg/docs/C3S/CDR3_2003-2018/PQAR/C3S_D312b_Lot2.2.3.2-v1.0_PQAR-GHG_ANNEX-D_v3.1.pdf, version 3.1, 03-11-2019.
- 815 Rodgers, C. D.: *Inverse Methods for Atmospheric Sounding: Theory and Practice*, World Scientific Publishing, Singapore, 2000.
- Rodgers, C. D. and Connor, B. J.: Intercomparison of remote sounding instruments, *J. Geophys. Res. Atmos.*, 108, 14, <https://doi.org/10.1029/2002jd002299>, <https://agupubs.onlinelibrary.wiley.com/doi/abs/10.1029/2002JD002299>, 2003.
- Schneising, O., Buchwitz, M., Burrows, J. P., Bovensmann, H., Reuter, M., Notholt, J., Macatangay, R., and Warneke, T.: Three years of greenhouse gas column-averaged dry air mole fractions retrieved from satellite - Part 1: Carbon dioxide, *Atmos. Chem. Phys.*, 8, 3827–
820 3853, <http://www.atmos-chem-phys.net/8/3827/2008/>, 2008.
- Schneising, O., Heymann, J., Buchwitz, M., Reuter, M., Bovensmann, H., and Burrows, J. P.: Anthropogenic carbon dioxide source areas observed from space: assessment of regional enhancements and trends, *Atmos. Chem. Phys.*, 13, 2445–2454, <https://doi.org/10.5194/acp-13-2445-2013>, <http://www.atmos-chem-phys.net/13/2445/2013/>, 2013.
- Schneising, O., Reuter, M., Buchwitz, M., Heymann, J., Bovensmann, H., and Burrows, J. P.: Terrestrial carbon sink observed from space: variation of growth rates and seasonal cycle amplitudes in response to interannual surface temperature variability, *Atmos. Chem. Phys.*,
825 14, 133–141, <https://doi.org/10.5194/acp-14-133-2014>, <http://www.atmos-chem-phys.net/14/133/2014/>, 2014.
- Schneising, O., Buchwitz, M., Reuter, M., Bovensmann, H., Burrows, J. P., Borsdorff, T., Deutscher, N. M., Feist, D. G., Griffith, D. W. T., Hase, F., Hermans, C., Iraci, L. T., Kivi, R., Landgraf, J., Morino, I., Notholt, J., Petri, C., Pollard, D. F., Roche, S., Shiomi, K., Strong,



- 830 K., Sussmann, R., Velazco, V. A., Warneke, T., and Wunch, D.: A scientific algorithm to simultaneously retrieve carbon monoxide and methane from TROPOMI onboard Sentinel-5 Precursor, *Atmos. Meas. Tech.*, 12, 6771–6802, <https://doi.org/10.5194/amt-12-6771-2019>, <https://amt.copernicus.org/articles/12/6771/2019/>, 2019.
- Schwandner, F. M., Gunson, M. R., Miller, C. E., Carn, S. A., Eldering, A., Krings, T., Verhulst, K. R., Schimel, D. S., Nguyen, H. M., Crisp, D., O'Dell, C. W., Osterman, G. B., Iraci, L. T., and Podolske, J. R.: Spaceborne detection of localized carbon dioxide sources, *Science*, 358, <https://doi.org/10.1126/science.aam5782>, <https://science.sciencemag.org/content/358/6360/eaam5782>, 2017.
- 835 Sherlock, V., Connor, B. J., Robinson, J., Shiona, H., Smale, D., and Pollard, D.: TCCON data from Lauder (NZ), 120HR, Release GGG2014R0, TCCON data archive, hosted by CaltechDATA, <https://doi.org/10.14291/tcon.ggg2014.lauder01.R0/1149293>, <https://tcondata.org>, 2014a.
- Sherlock, V., Connor, B. J., Robinson, J., Shiona, H., Smale, D., and Pollard, D.: TCCON data from Lauder (NZ), 125HR, Release GGG2014R0, TCCON data archive, hosted by CaltechDATA, <https://doi.org/10.14291/tcon.ggg2014.lauder02.R0/1149298>, <https://tcondata.org>, 2014b.
- 840 Strong, K., Roche, S., Franklin, J. E., Mendonca, J., Lutsch, E., Weaver, D., Fogal, P. F., Drummond, J. R., Batchelor, R., and Lindenmaier, R.: TCCON data from Eureka (CA), Release GGG2014.R3, <https://doi.org/10.14291/TCCON.GGG2014.EUREKA01.R3>, <https://data.caltech.edu/records/1171>, 2019.
- Sussmann, R. and Rettinger, M.: TCCON data from Garmisch (DE), Release GGG2014.R2, <https://doi.org/10.14291/TCCON.GGG2014.GARMISCH01.R2>, <https://data.caltech.edu/records/956>, 2018a.
- 845 Sussmann, R. and Rettinger, M.: TCCON data from Zugspitze (DE), Release GGG2014R1, TCCON data archive, hosted by CaltechDATA, <https://doi.org/10.14291/tcon.ggg2014.zugspitze01.R1>, <https://tcondata.org>, 2018b.
- Suto, H., Kataoka, F., Kikuchi, N., Knuteson, R. O., Butz, A., Haun, M., Buijs, H., Shiomi, K., Imai, H., and Kuze, A.: Thermal and near-infrared sensor for carbon observation Fourier-transform spectrometer-2 (TANSO-FTS-2) on the Greenhouse Gases Observing Satellite-2 (GOSAT-2) during its first year on orbit, *Atmos. Meas. Tech. Discuss.*, 2020, 1–51, <https://doi.org/10.5194/amt-2020-360>, <https://amt.copernicus.org/preprints/amt-2020-360/>, 2020.
- 850 Te, Y., Jeseck, P., and Janssen, C.: TCCON data from Paris (FR), Release GGG2014R0, TCCON data archive, hosted by CaltechDATA, <https://doi.org/10.14291/tcon.ggg2014.paris01.R0/1149279>, <https://tcondata.org>, 2014.
- Warneke, T., Messerschmidt, J., Notholt, J., Weinzierl, C., Deutscher, N. M., Petri, C., and Grupe, P.: TCCON data from Orléans (FR), Release GGG2014.R1, <https://doi.org/10.14291/TCCON.GGG2014.ORLEANS01.R1>, <https://data.caltech.edu/records/1301>, 2019.
- 855 Wennberg, P. O., Wunch, D., Roehl, C., Blavier, J.-F., Toon, G. C., and Allen, N.: TCCON data from Caltech (US), Release GGG2014R1, TCCON data archive, hosted by CaltechDATA, <https://doi.org/10.14291/tcon.ggg2014.pasadena01.R1/1182415>, <https://tcondata.org>, 2014.
- Wennberg, P. O., Wunch, D., Roehl, C., Blavier, J.-F., Toon, G. C., Allen, N., Dowell, P., Teske, K., Martin, C., and Martin, J.: TCCON data from Lamont (US), Release GGG2014R1, TCCON data archive, hosted by CaltechDATA, <https://doi.org/10.14291/tcon.ggg2014.lamont01.R1/1255070>, <https://tcondata.org>, 2016.
- 860 Wennberg, P. O., Roehl, C. M., Wunch, D., Toon, G. C., Blavier, J.-F., Washenfelder, R., Keppel-Aleks, G., Allen, N. T., and Ayers, J.: TCCON data from Park Falls (US), Release GGG2014.R1, <https://doi.org/10.14291/TCCON.GGG2014.PARKFALLS01.R1>, <https://data.caltech.edu/records/295>, 2017.
- 865 Wu, D., Lin, J. C., Oda, T., and Kort, E. A.: Space-based quantification of per capita CO₂ emissions from cities, *Environ. Res. Lett.*, 15, 035 004, <https://doi.org/10.1088/1748-9326/ab68eb>, <https://iopscience.iop.org/article/10.1088/1748-9326/ab68eb>, 2020.



- Wunch, D., Toon, G. C., Wennberg, P. O., Wofsy, S. C., Stephens, B. B., Fischer, M. L., Uchino, O., Abshire, J. B., Bernath, P., Biraud, S. C., Blavier, J. F. L., Boone, C., Bowman, K. P., Browell, E. V., Campos, T., Connor, B. J., Daube, B. C., Deutscher, N. M., Dia, M., Elkins, J. W., Gerbig, C., Gottlieb, E., Griffith, D. W. T., Hurst, D. F., Jiménez, R., Keppel-Aleks, G., Kort, E. A., Macatangay, R., 870 Machida, T., Matsueda, H., Moore, F., Morino, I., Park, S., Robinson, J., Roehl, C. M., Sawa, Y., Sherlock, V., Sweeney, C., Tanaka, T., and Zondlo, M. A.: Calibration of the Total Carbon Column Observing Network using aircraft profile data, *Atmos. Meas. Tech.*, 3, 1351–1362, <https://doi.org/10.5194/amt-3-1351-2010>, <http://www.atmos-meas-tech.net/3/1351/2010/>, 2010.
- Wunch, D., Toon, G. C., Blavier, J.-F. L., Washenfelder, R. A., Notholt, J., Connor, B. J., Griffith, D. W. T., Sherlock, V., and Wennberg, P. O.: The Total Carbon Column Observing Network, *Phil. Trans. R. Soc. A*, 369, 2087–2112, <https://doi.org/10.1098/rsta.2010.0240>, 875 <https://royalsocietypublishing.org/doi/abs/10.1098/rsta.2010.0240>, 2011.
- Wunch, D., Mendonca, J., Colebatch, O., Allen, N., Blavier, J.-F. L., Roche, S., Hedelius, J. K., Neufeld, G., Springett, S., Worthy, D. E. J., Kessler, R., and Strong, K.: TCCON data from East Trout Lake (CA), Release GGG2014R1, TCCON data archive, hosted by CaltechDATA, <https://doi.org/10.14291/tcon.ggg2014.easttroutlake01.R1>, <https://tccodata.org>, 2017.
- Yang, D., Liu, Y., Cai, Z., Chen, X., Yao, L., and Lu, D.: First Global Carbon Dioxide Maps Produced from TanSat Measurements, *Adv. Space Res.*, 35, 621–623, <https://doi.org/10.1007/s00376-018-7312-6>, <https://doi.org/10.1007/s00376-018-7312-6>, 2018. 880
- Yin, Y., Ciais, P., Chevallier, F., Li, W., Bastos, A., Piao, S., Wang, T., and Liu, H.: Changes in the Response of the Northern Hemisphere Carbon Uptake to Temperature Over the Last Three Decades, *Geophys. Res. Lett.*, 45, 4371–4380, <https://doi.org/10.1029/2018GL077316>, <https://agupubs.onlinelibrary.wiley.com/doi/abs/10.1029/2018GL077316>, 2018.
- Zheng, B., Chevallier, F., Ciais, P., Broquet, G., Wang, Y., Lian, J., and Zhao, Y.: Observing carbon dioxide emissions over China's cities with the Orbiting Carbon Observatory-2, *Atmos. Chem. Phys. Discuss.*, 2020, 1–17, <https://doi.org/10.5194/acp-2020-123>, <https://www.atmos-chem-phys-discuss.net/acp-2020-123/>, 2020. 885

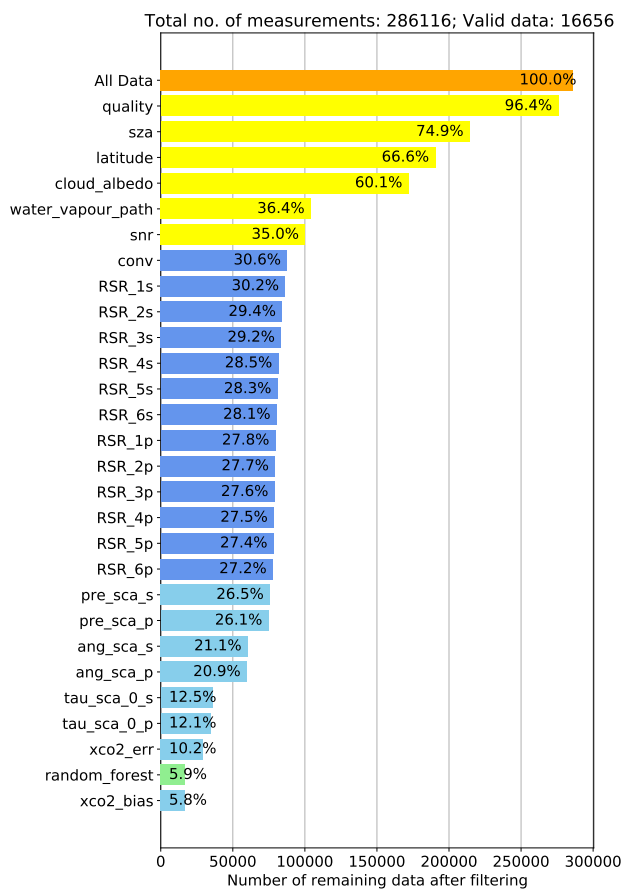


Figure 1. Example for GOSAT data filtering during the different processing steps (April 2019). Filters are listed in sequential order from top to bottom on the vertical axis. Numbers in the horizontal bars denote the percentage of remaining data after this filter was applied. Orange: Total number of measurements before filtering. Yellow: Pre-processing filters. Blue: Step 1 post-processing filters (convergence and noise). Green: Random forest post-processing filter. Light blue: Additional post-processing filters.

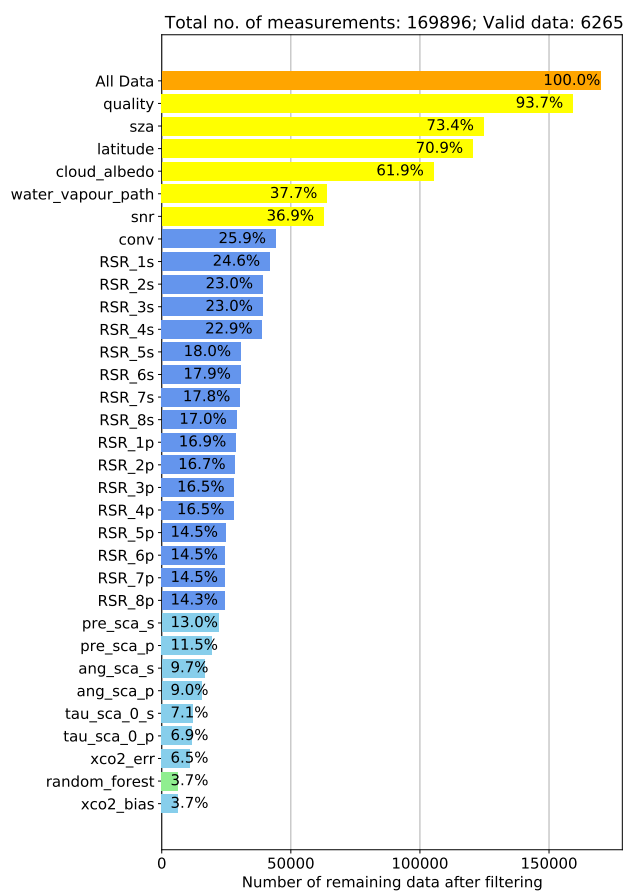


Figure 2. Same as Fig. 1, but for GOSAT-2.

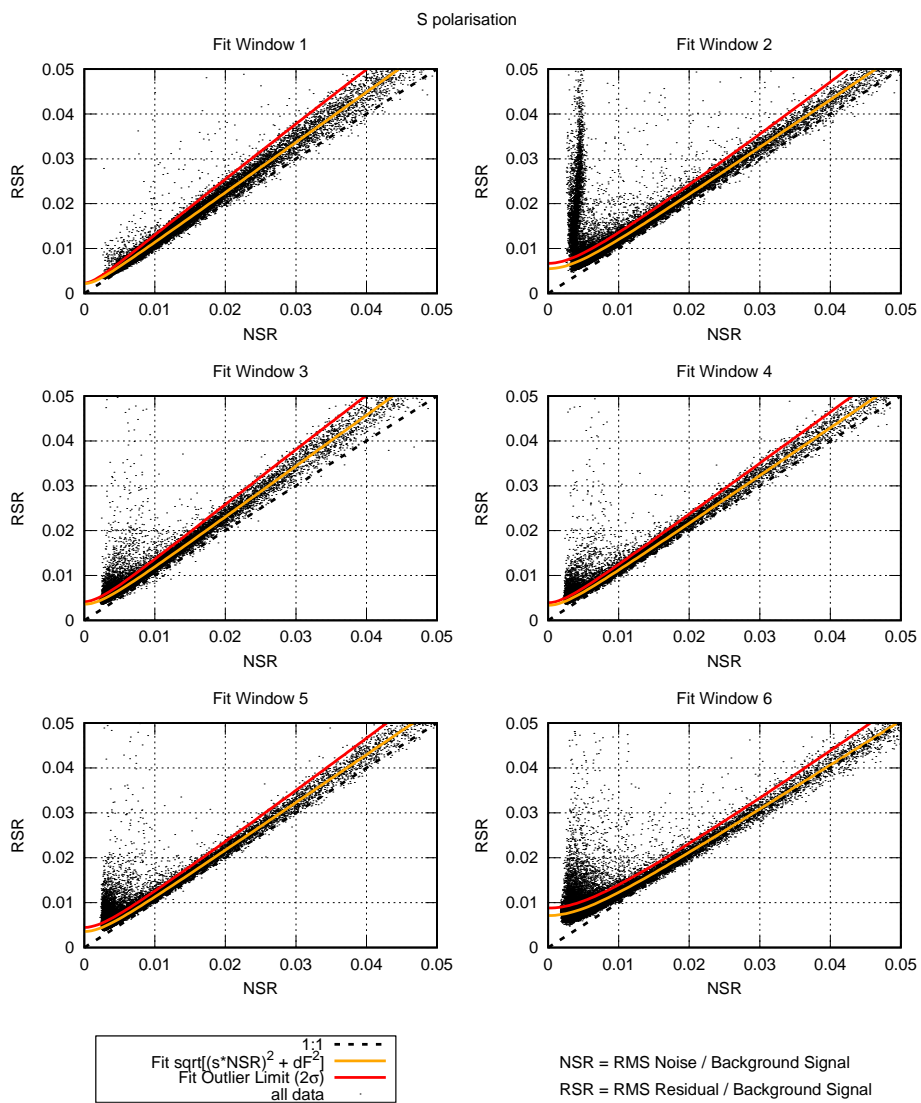


Figure 3. GOSAT noise model (S polarisation).

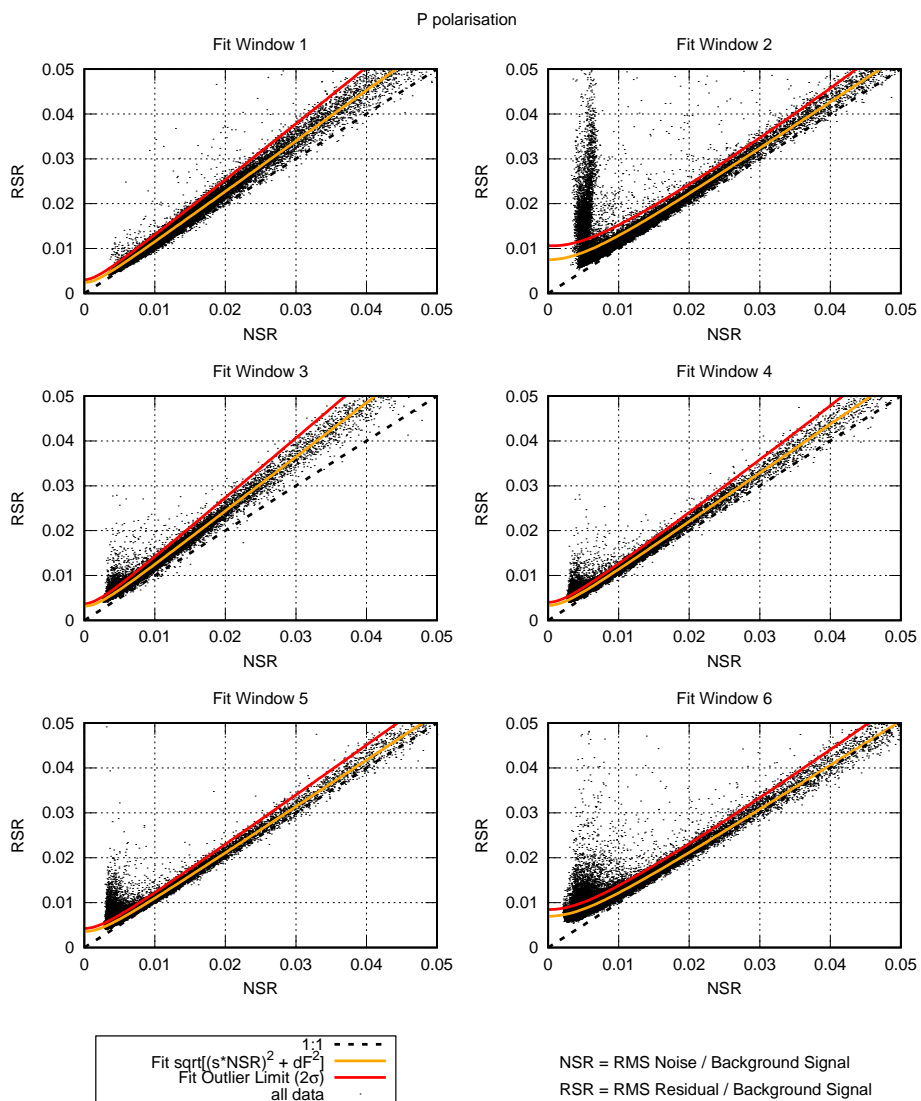


Figure 4. GOSAT noise model (P polarisation).

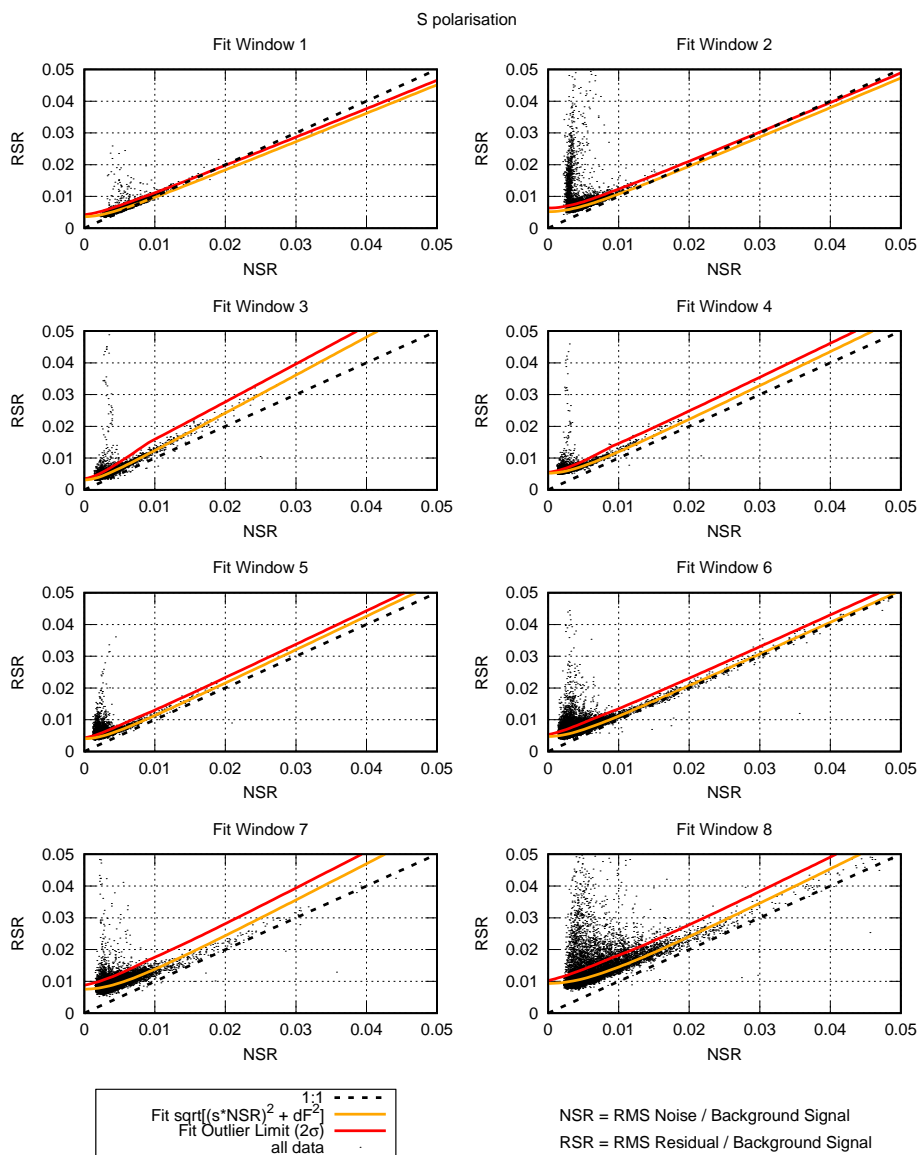


Figure 5. GOSAT-2 noise model (S polarisation).

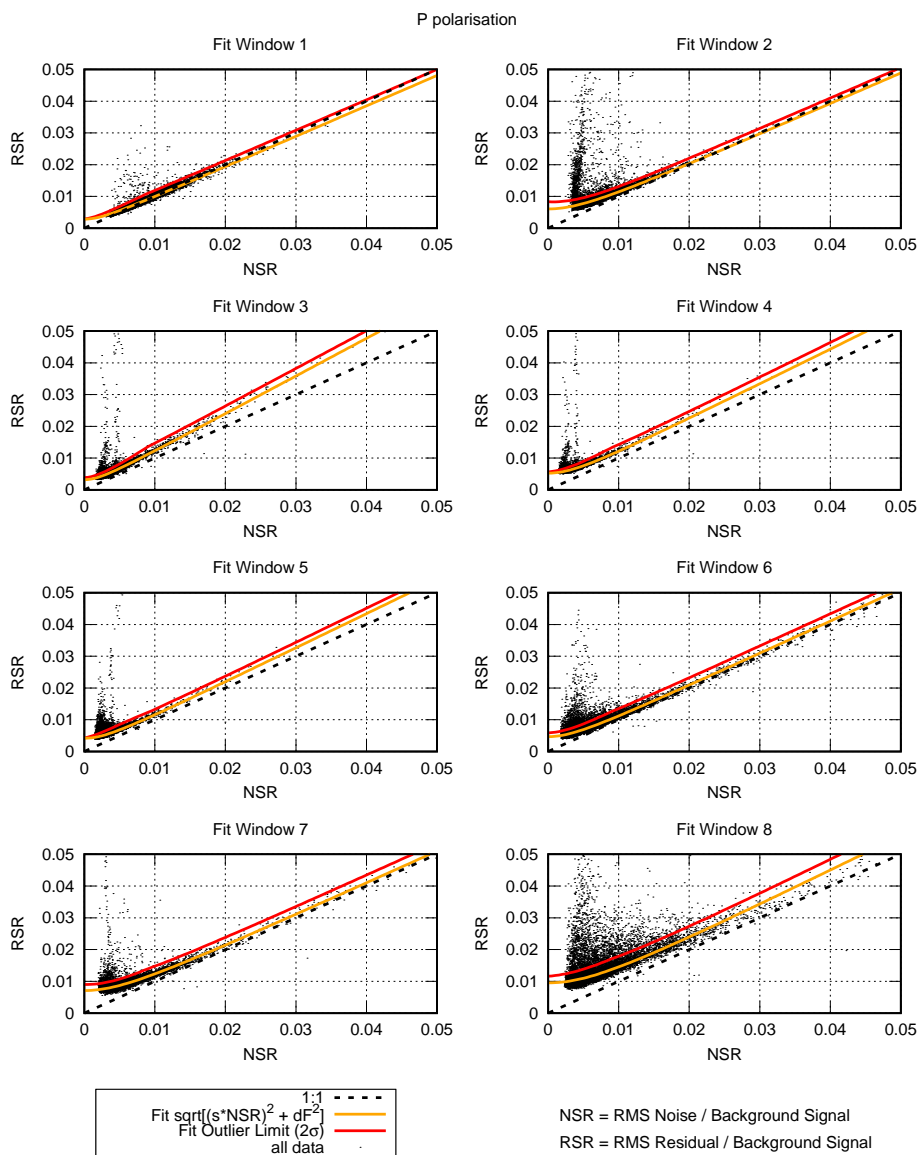


Figure 6. GOSAT-2 noise model (P polarisation).

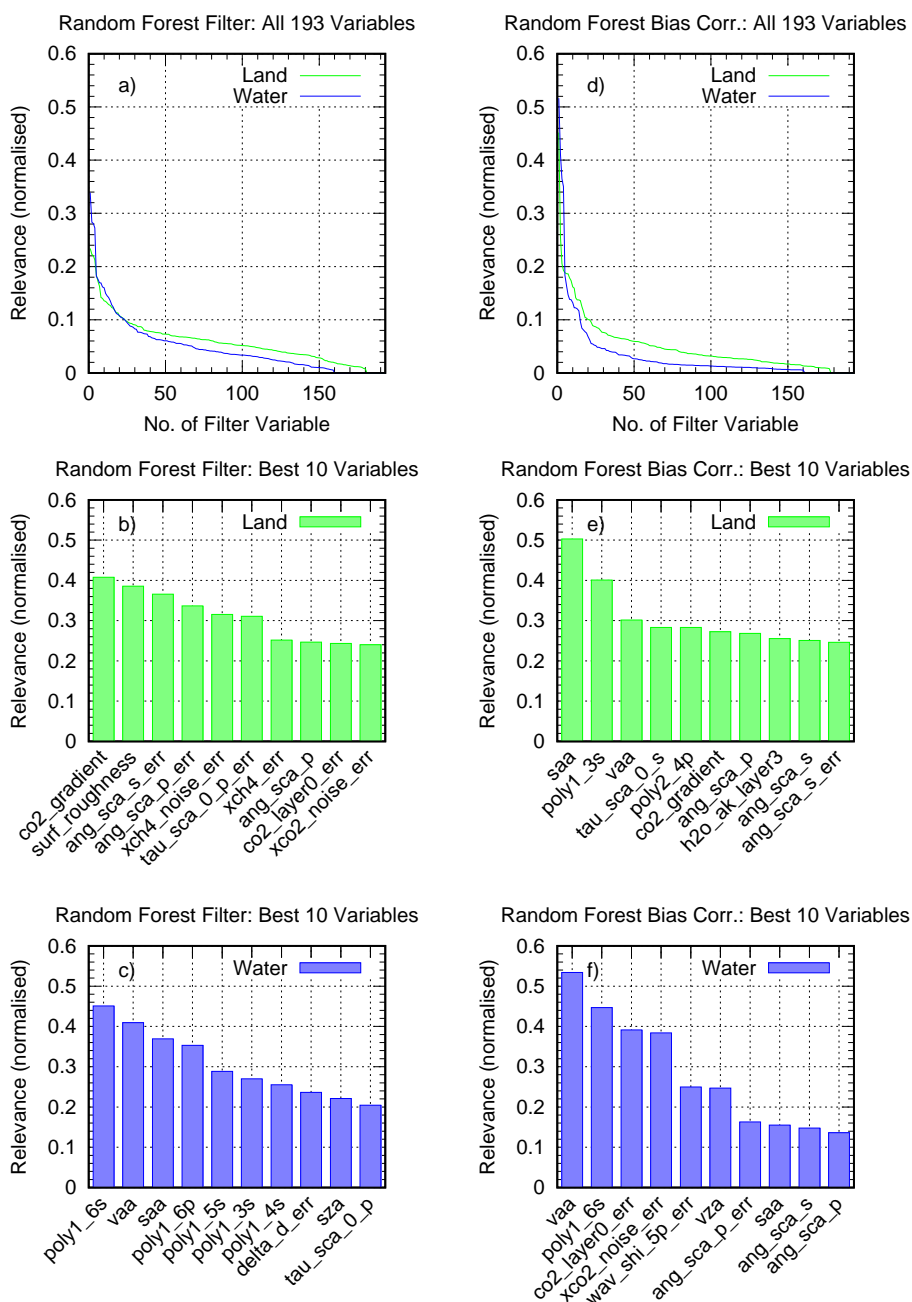


Figure 7. Random forest results for GOSAT. Left (a–c): Results from random forest filter. Right (d–f): Results from random forest bias correction. Top: Normalised relevance (score) of all filter variables. Middle/bottom: Selected variables and their relevance for land/water surface.

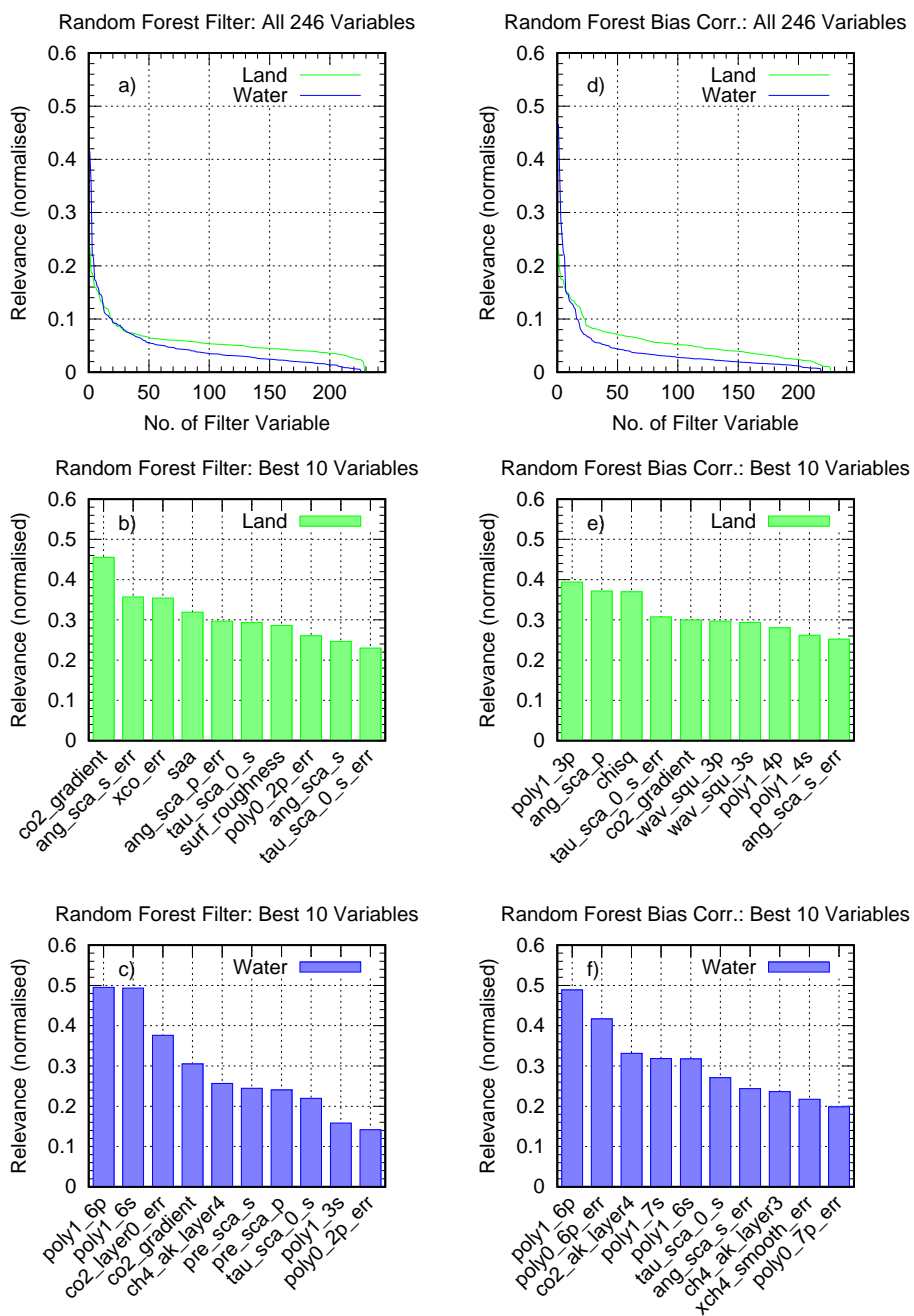


Figure 8. As Fig. 7, but for GOSAT-2.

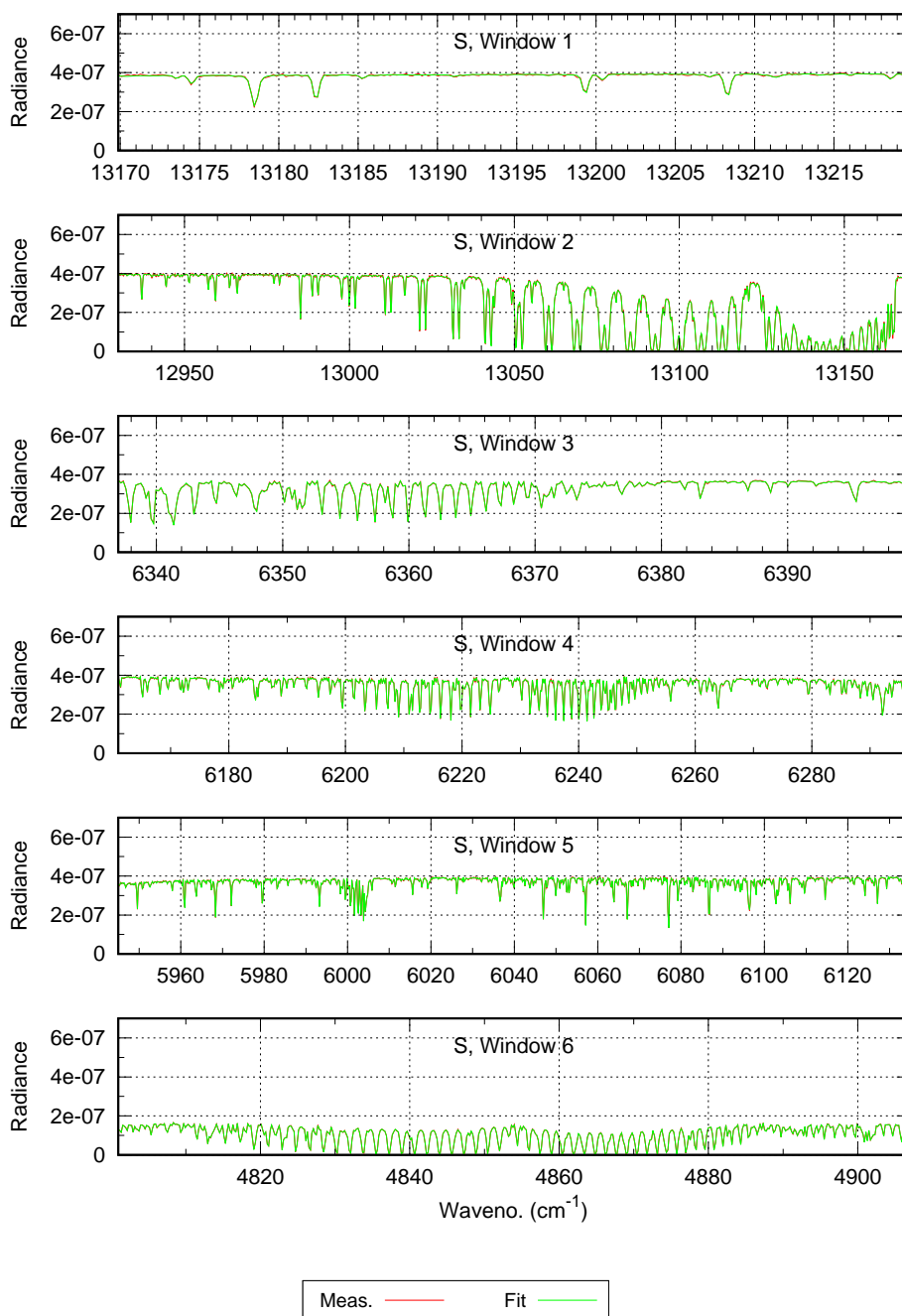


Figure 9. Example for a single GOSAT measurement (S polarisation): Measured (red) and retrieved (green) spectra in the different fit windows; because of the good agreement the red curve is essentially barely visible below the green curve. Radiance unit is $\text{W/cm}^2/\text{cm}^{-1}/\text{sr}$.

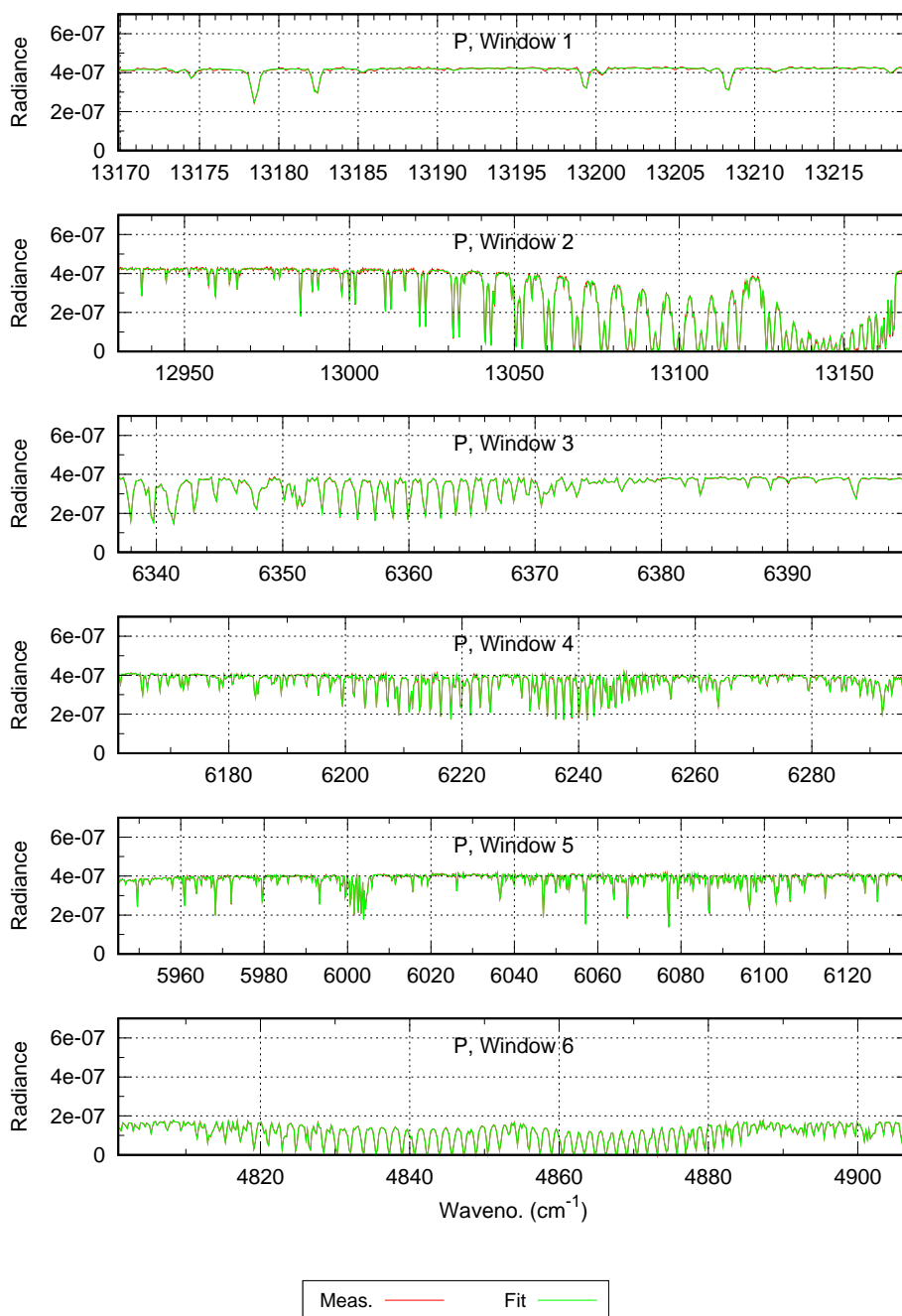


Figure 10. Same as Fig. 9 but for P polarisation.

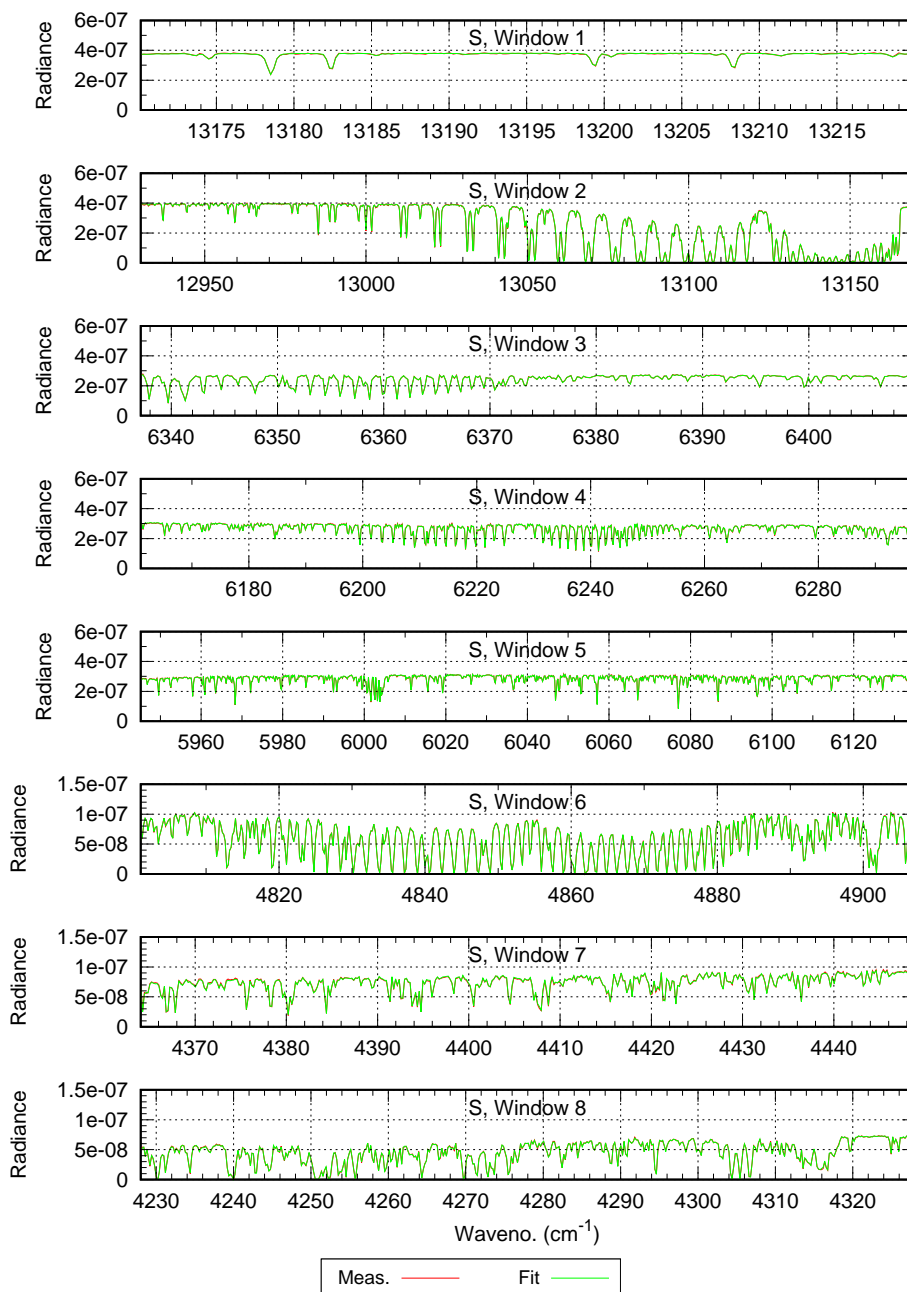


Figure 11. Same as Fig. 9 but for GOSAT-2 with two additional fit windows.

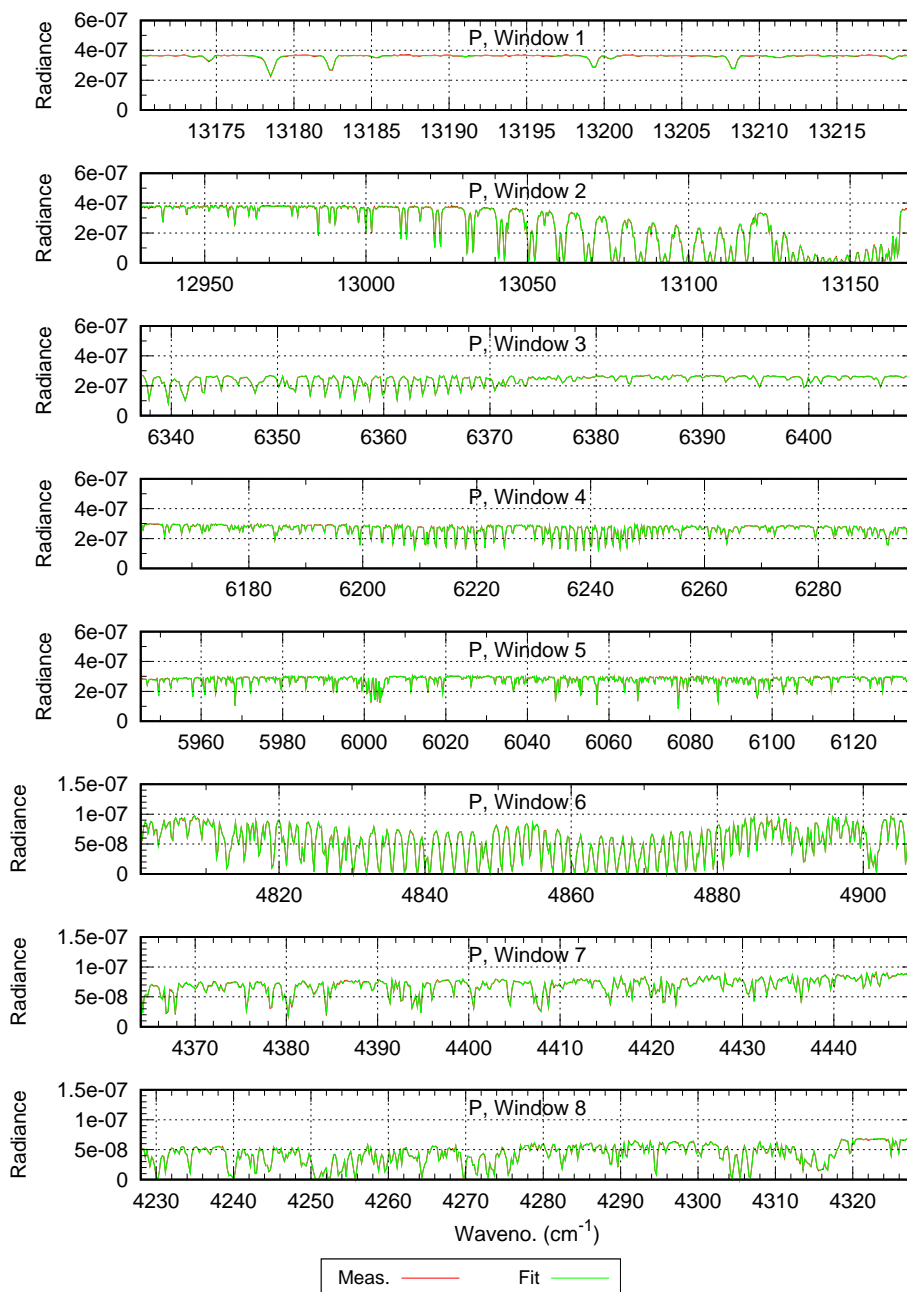


Figure 12. Same as Fig. 11 but for P polarisation.

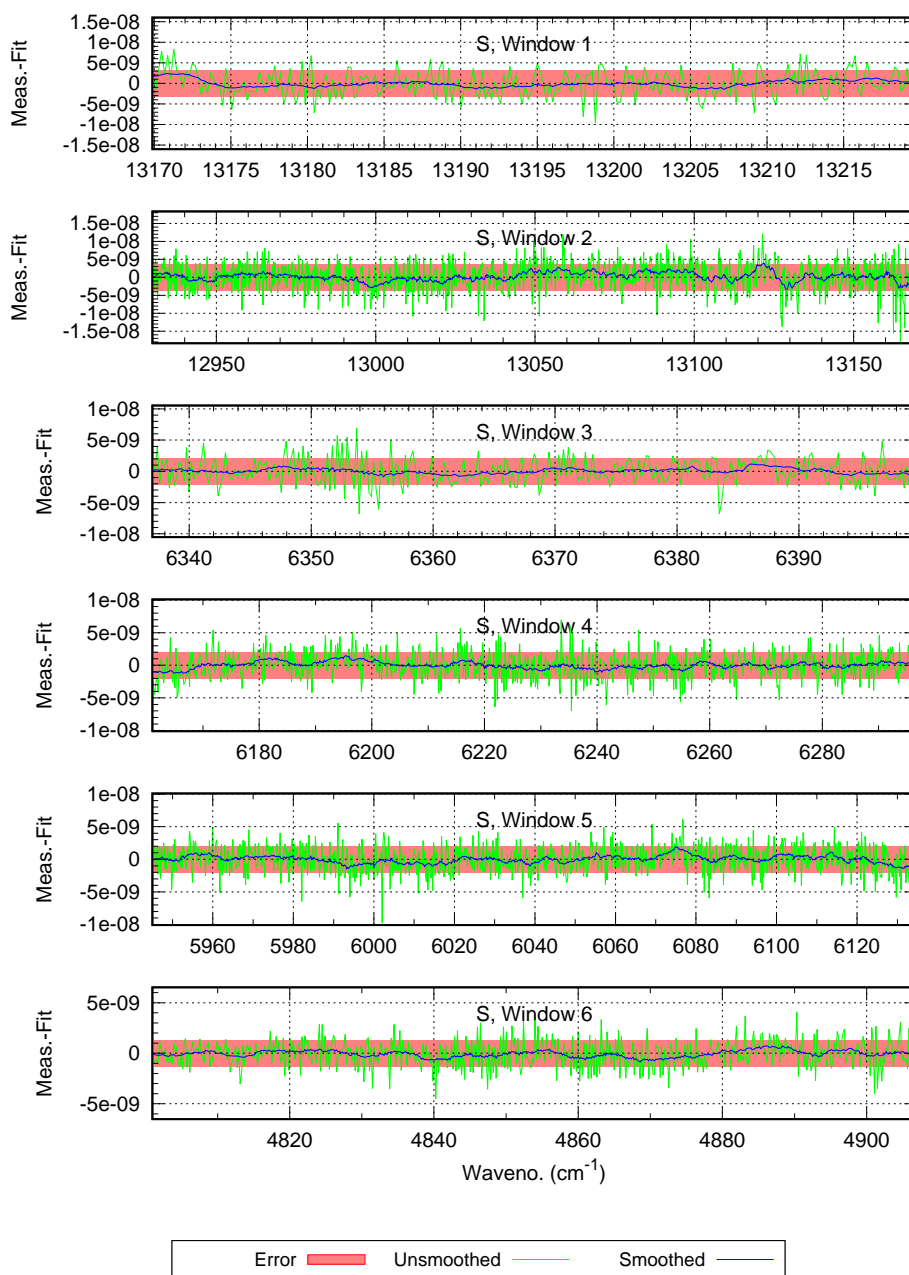


Figure 13. GOSAT residuals (measurement - fit) for data from Fig. 9 (S polarisation). Green: Unsmoothed. Blue: Smoothed with a boxcar of width 21 spectral pixels ($= 4.2 \text{ cm}^{-1}$). Red: Estimated noise error range. Radiance difference unit is $\text{W}/\text{cm}^2/\text{cm}^{-1}/\text{sr}$.

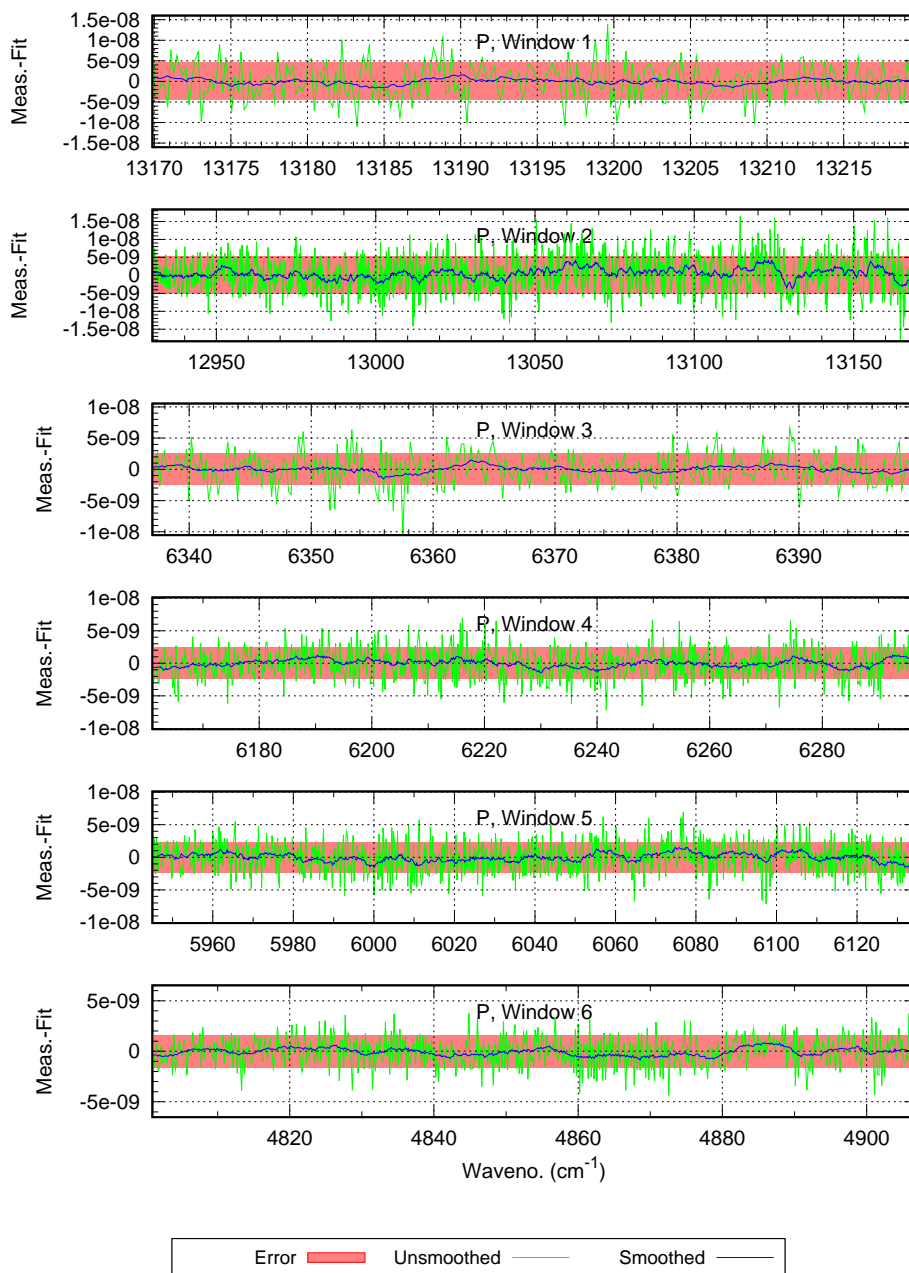


Figure 14. Same as Fig. 13 but for P polarisation.

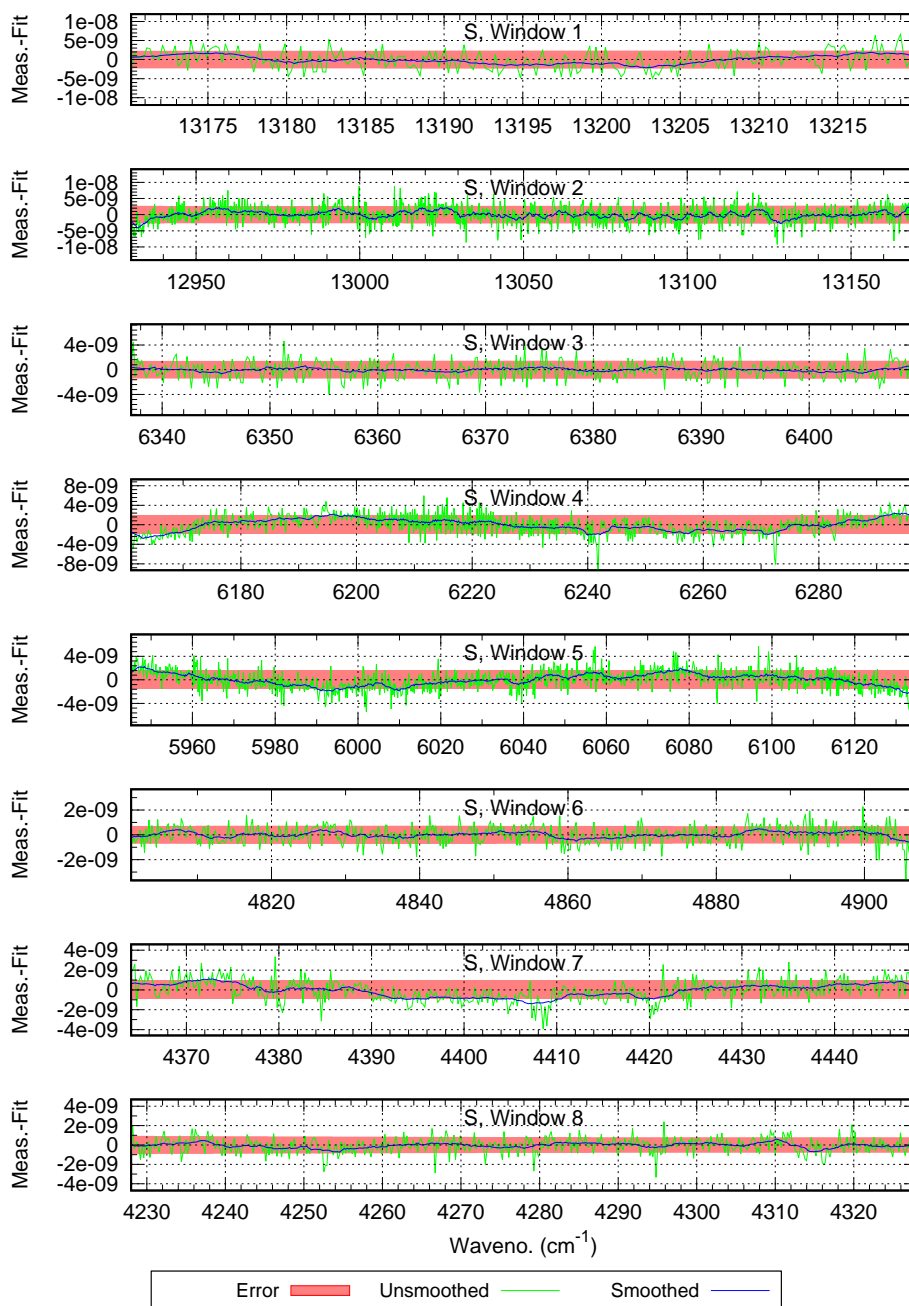


Figure 15. Same as Fig. 13 but for GOSAT-2.

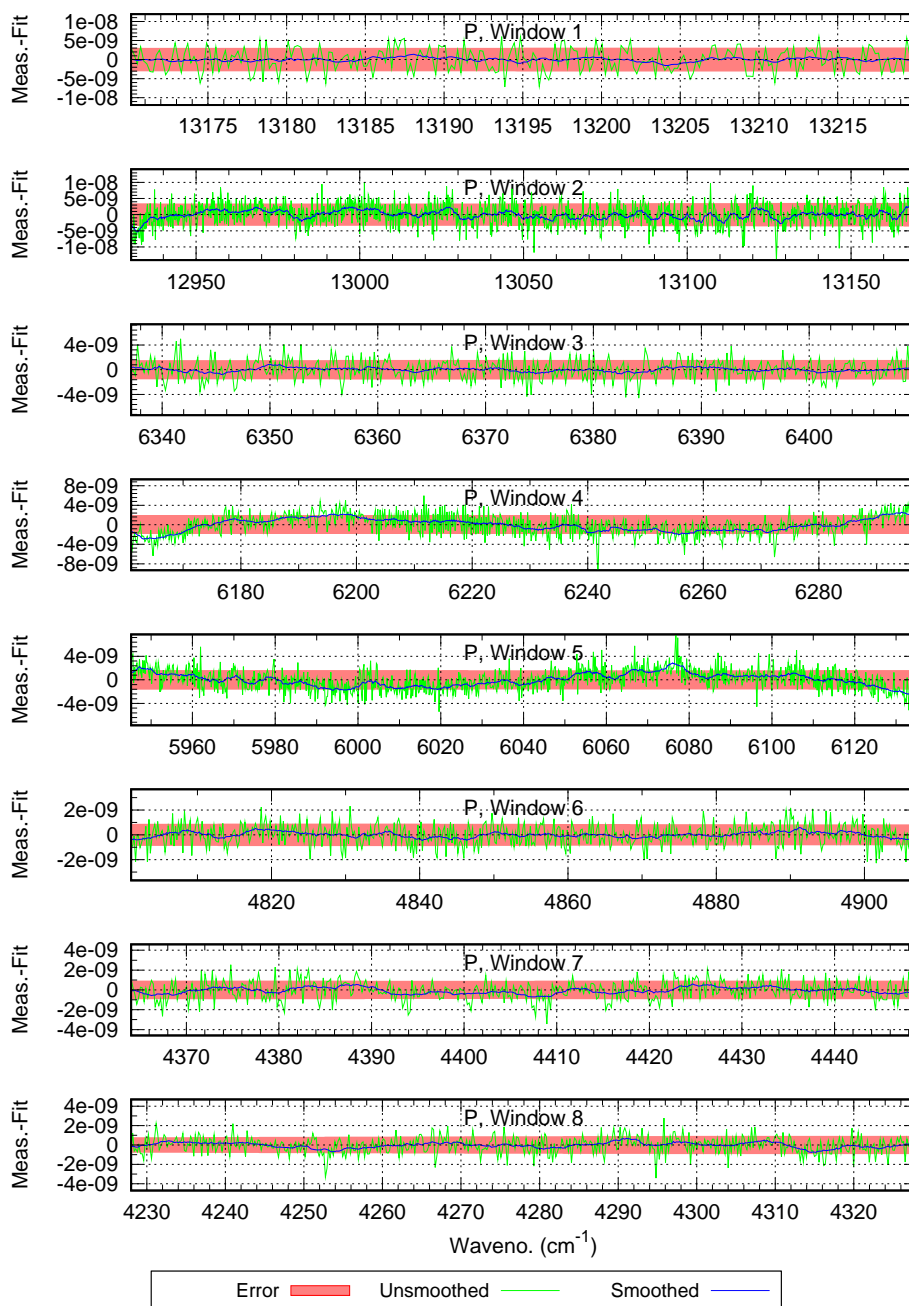


Figure 16. Same as Fig. 14 but for GOSAT-2.

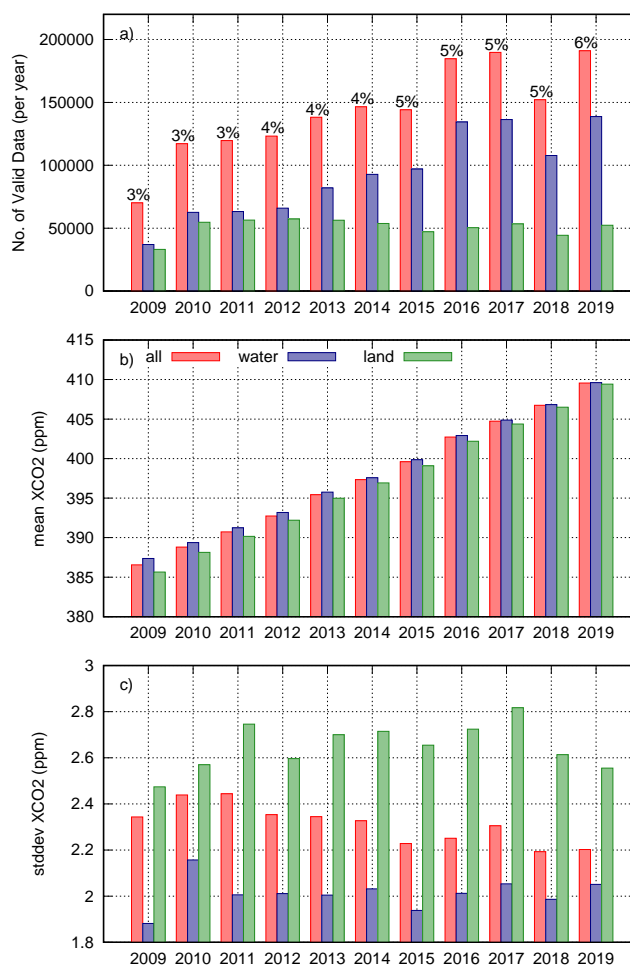


Figure 17. Statistics for valid GOSAT measurements (after pre- and post-processing filtering) for each year. Blue: Measurements over water. Green: Measurements over land. Red: All data. a) Number of valid measurements, incl. percentage of all originally available measurements. b) Global mean XCO₂. c) Corresponding standard deviation.

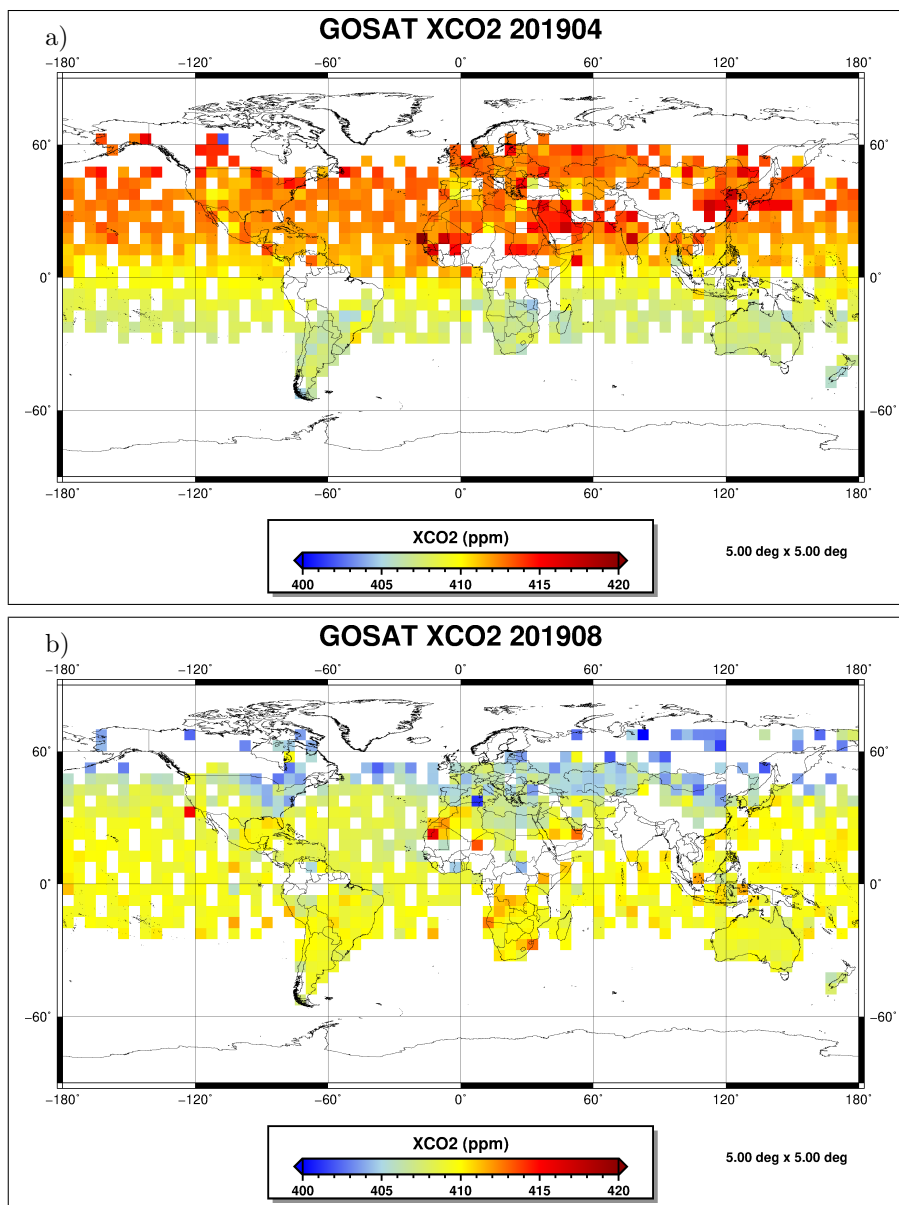


Figure 18. Example for gridded GOSAT XCO₂ data. a) April 2019. b) August 2019.

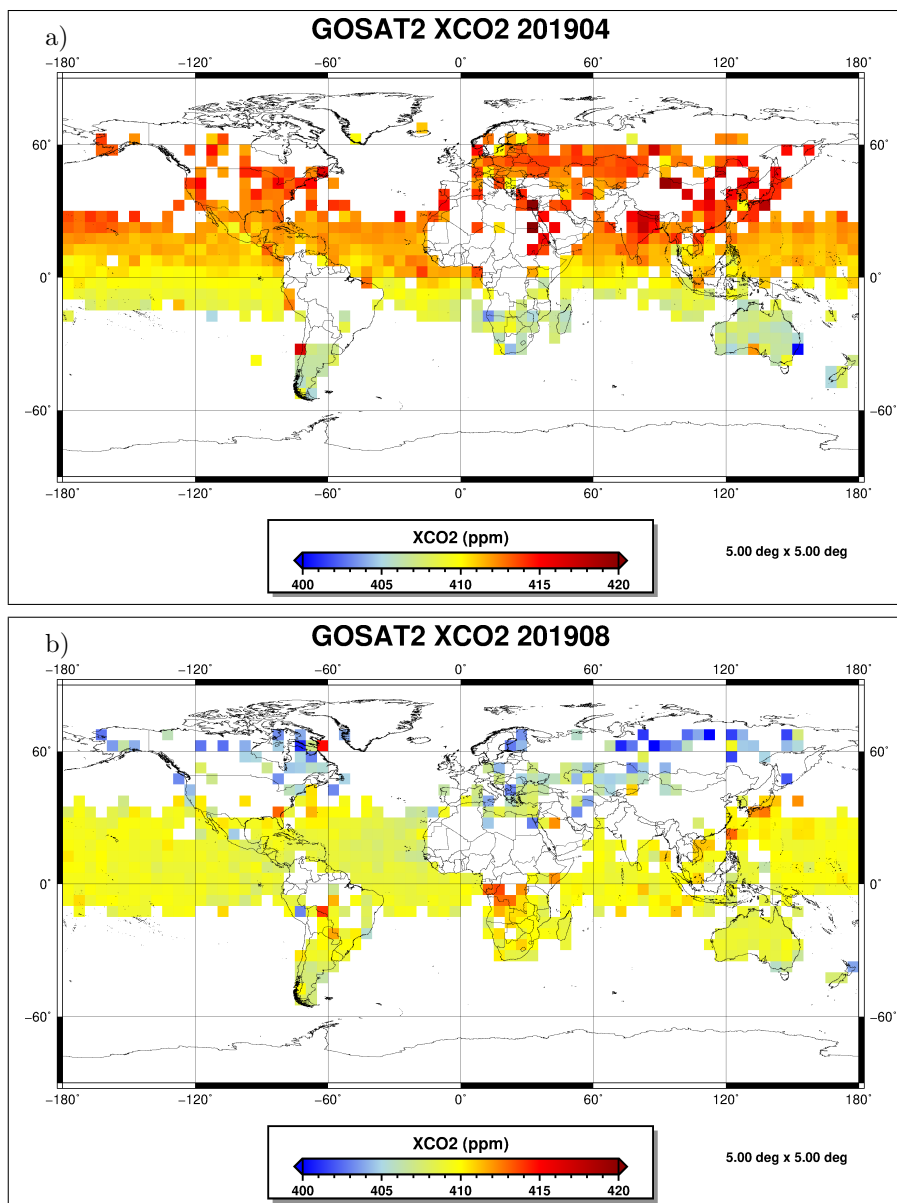


Figure 19. Example for gridded GOSAT-2 XCO₂ data. a) April 2019. b) August 2019.

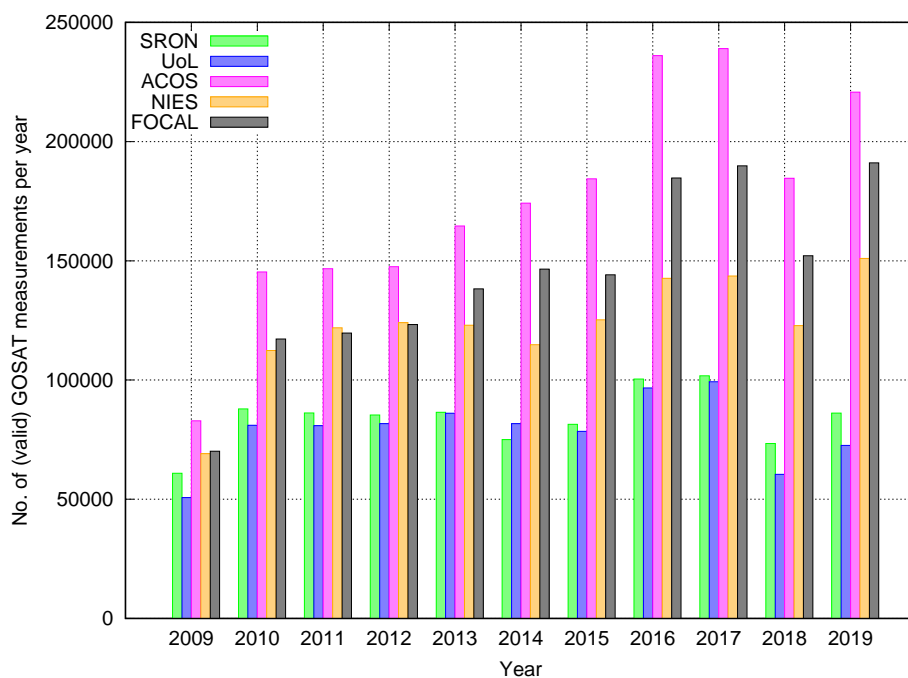


Figure 20. Number of valid XCO₂ data points in the different GOSAT products from 2009 to 2019.

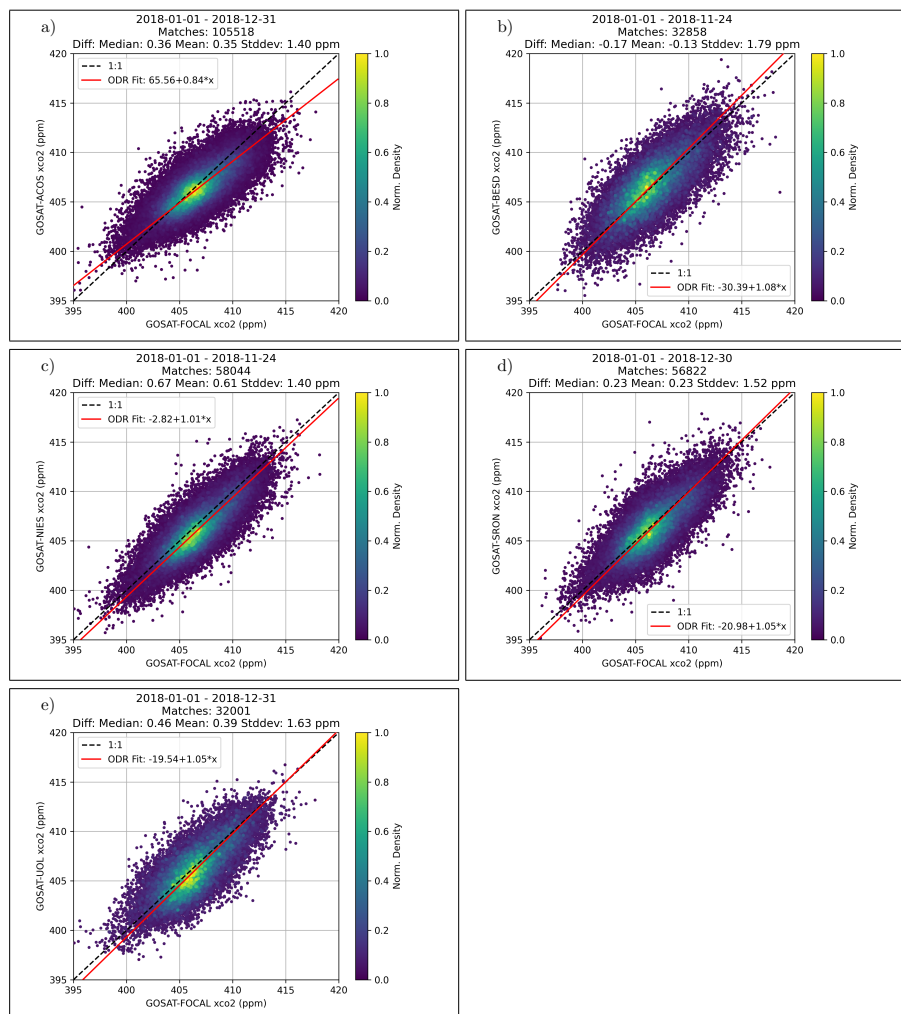


Figure 21. Comparison of GOSAT-FOCAL data (x axis) from 2018 with other GOSAT data (y axis). The colour of the data points corresponds to the density of data points at that location (normalised to a maximum value of 1). The dashed line corresponds to perfect agreement. The red line shows the result of a linear fit using the Orthogonal Distance Regression (ODR) method. The total number of collocated data as well as median, mean and standard deviation of the XCO₂ differences between the two data sets are given in the title of the sub-plots. a) FOCAL vs. ACOS b) FOCAL vs. BESD. c) FOCAL vs. NIES. d) FOCAL vs. SRON. e) FOCAL vs. UoL.

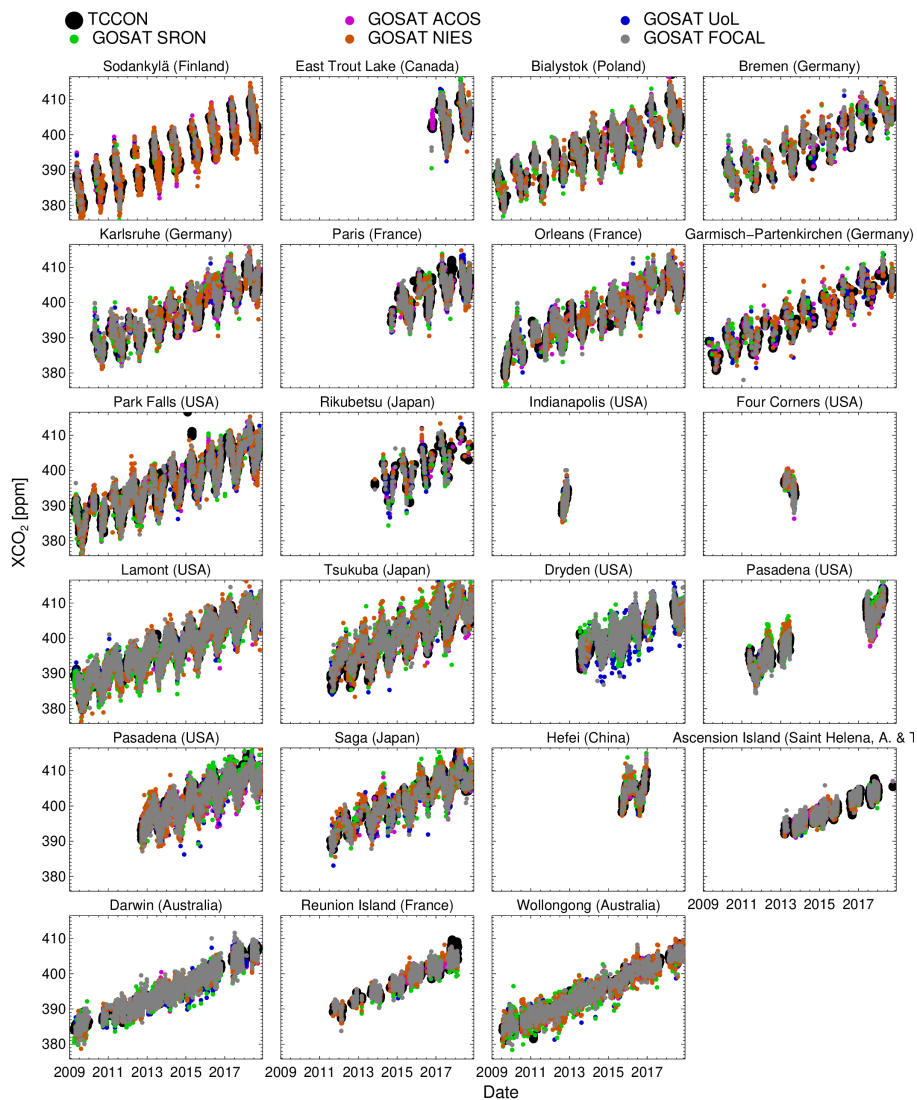


Figure 22. Time series of collocated GOSAT data at various TCCON sites for different data products including the new GOSAT-FOCAL data set.

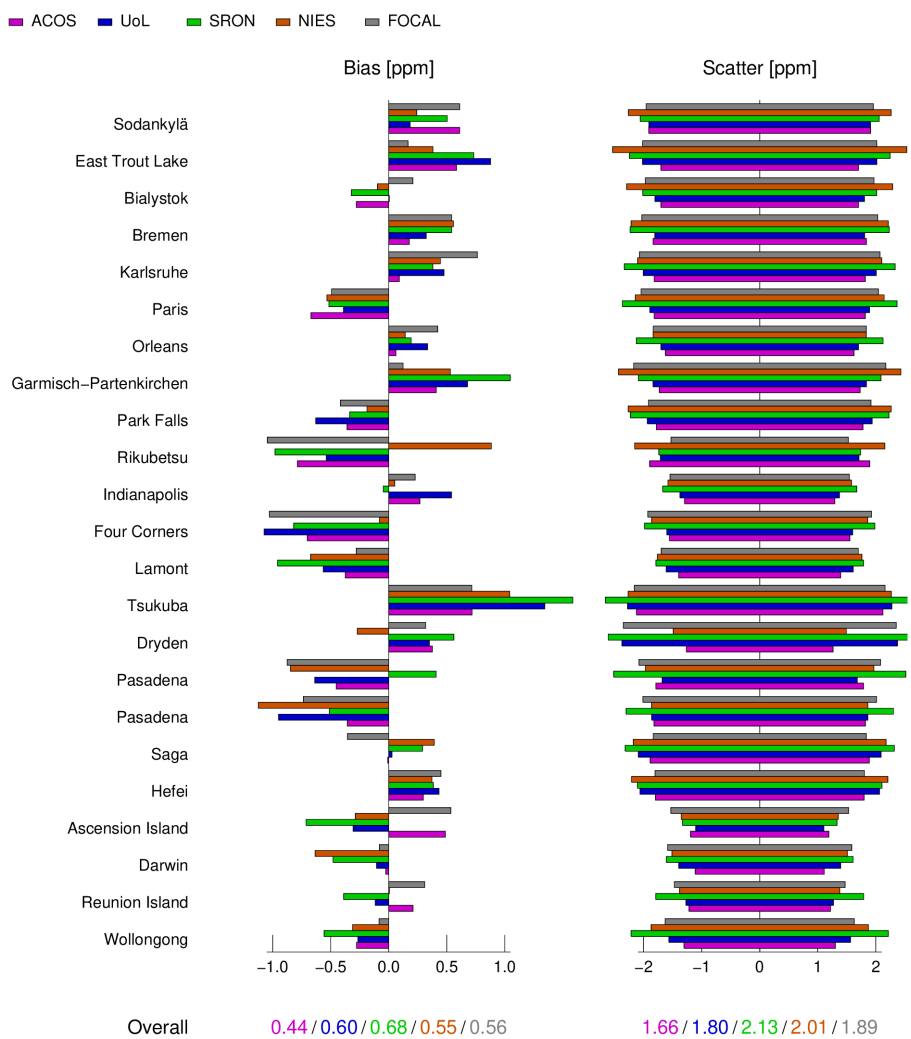


Figure 23. Overview of TCCON validation results.

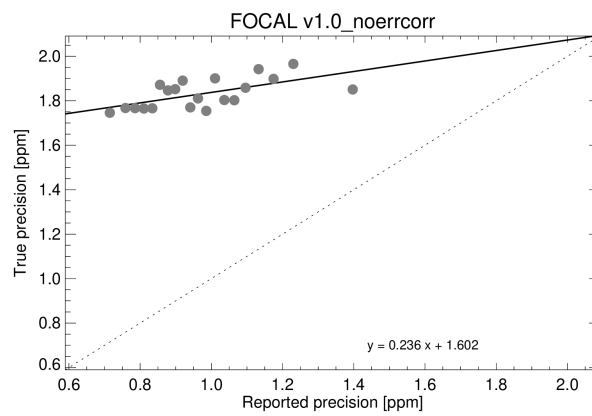


Figure 24. Comparisons of the (binned) original XCO₂ errors (reported precision without correction) of the GOSAT-FOCAL product with estimated errors based on collocated TCCON data (true precision).

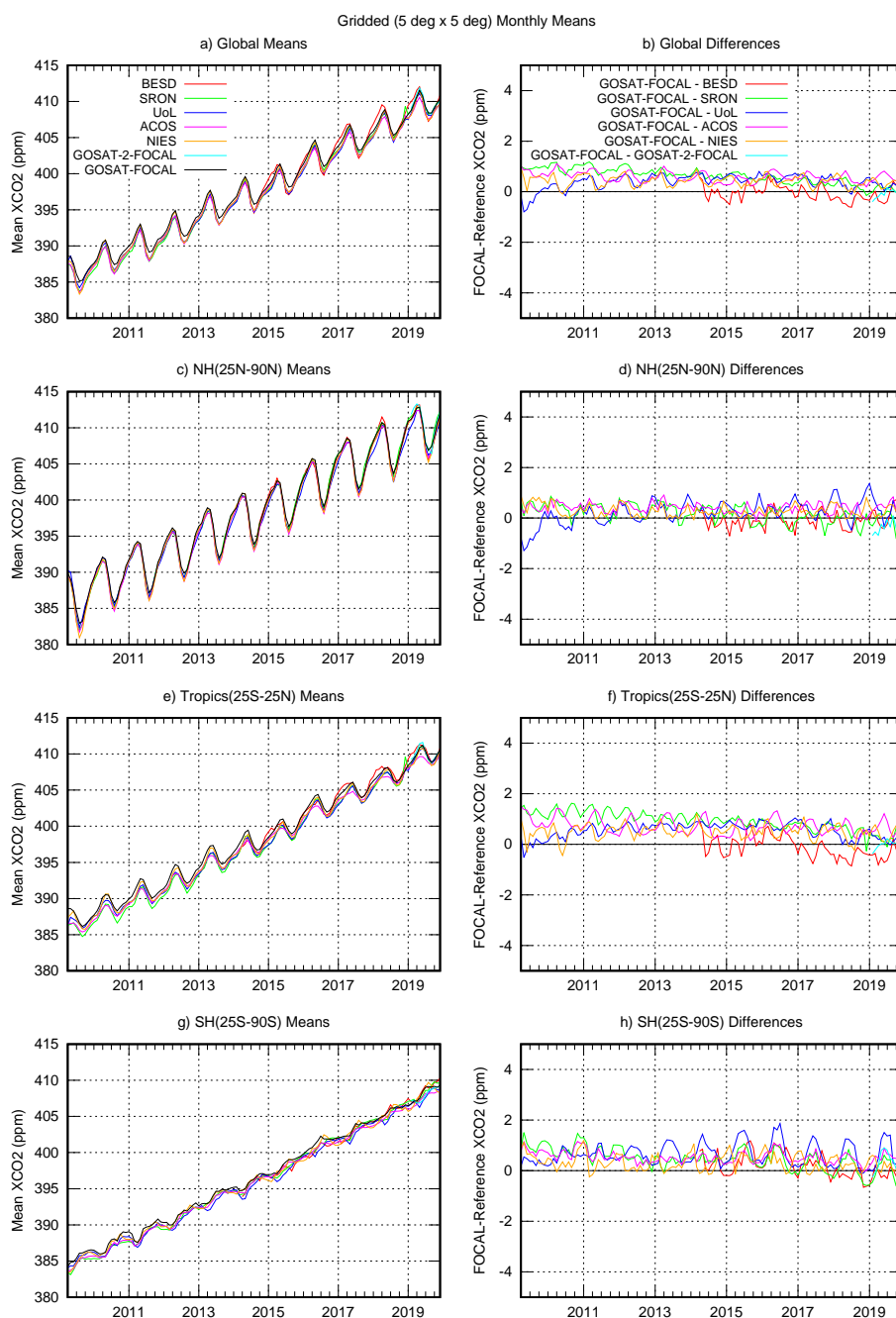


Figure 25. Gridded monthly mean time series of different GOSAT XCO₂ products. Left: Time series of mean XCO₂ for four different regions (from top to bottom: Global, northern hemisphere, tropics, southern hemisphere). Right: Corresponding differences to the GOSAT-FOCAL product.



Table 1. TCCON stations used in this study.

Site	Lon. (deg)	Lat. (deg)	Elev. (km)	Reference(s)
Ascension Island (SH)	-14.33	-7.92	0.01	Feist et al. (2014)
Bialystok (PL)	23.03	53.23	0.18	Deutscher et al. (2019)
Bremen (DE)	8.85	53.10	0.04	Notholt et al. (2019a)
Burgos (PH)	120.65	18.53	0.04	Morino et al. (2018b)
Darwin (AU)	130.89	-12.42	0.03	Griffith et al. (2014a)
Edwards (US)	-117.88	34.96	0.70	Iraci et al. (2016a)
East Trout Lake (CA)	-104.99	54.35	0.50	Wunch et al. (2017)
Eureka (CA)	-86.42	80.05	0.61	Strong et al. (2019)
Four Corners (US)	-108.48	36.80	1.64	Dubey et al. (2014)
Garmisch-Partenkirchen (DE)	11.06	47.48	0.74	Sussmann and Rettinger (2018a)
Hefei (CN)	117.17	31.90	0.04	Liu et al. (2018)
Indianapolis (US)	-86.00	39.86	0.27	Iraci et al. (2016b)
Izaña (ES)	-16.50	28.30	2.37	Blumenstock et al. (2017)
Karlsruhe (DE)	8.43	49.10	0.11	Hase et al. (2014)
Lamont (US)	-97.49	36.60	0.32	Wennberg et al. (2016)
Lauder (NZ)	169.68	-45.04	0.37	Sherlock et al. (2014a, b) Pollard et al. (2019)
Ny Ålesund (NO)	11.90	78.90	0.02	Notholt et al. (2019b)
Orleans (FR)	2.11	47.97	0.13	Warneke et al. (2019)
Paris (FR)	2.36	48.85	0.06	Te et al. (2014)
Park Falls (US)	-90.27	45.95	0.44	Wennberg et al. (2017)
Pasadena (US)	-118.13	34.13	0.21	Wennberg et al. (2014)
Reunion Island (FR)	55.49	-20.90	0.09	De Mazière et al. (2017)
Rikubetsu (JP)	143.77	43.46	0.36	Morino et al. (2017)
Saga (JP)	130.29	33.24	0.01	Kawakami et al. (2014)
Sodankylä (FI)	26.63	67.37	0.18	Kivi et al. (2014)
Tsukuba (JP)	140.12	36.05	0.03	Morino et al. (2018a)
Wollongong (AU)	150.88	-34.41	0.03	Griffith et al. (2014b)
Zugspitze (DE)	10.98	47.42	2.96	Sussmann and Rettinger (2018b)



Table 2. Pre-processing filter limits.

Filter	Value
GOSAT quality flag	“good” or “poor”
GOSAT-2 quality flag	“good”, “fair” or “poor”
Maximum solar zenith angle	70°
Maximum latitude	70°
Minimum SNR	10
Maximum cloud albedo	0.7
Maximum water vapour path	4.0



Table 3. Parameters for cloud filtering.

Cloud Albedo		
GOSAT Band	Waveno. Range (cm^{-1})	Irradiance ($\text{W}/\text{cm}^2/\text{s}/\text{cm}^{-1}$)
SWIR-1	13190–13210	7.4e-6
SWIR-2	6267–6279	6.0e-6
SWIR-3	4800–4810	4.3e-6

Water Vapour Path	
GOSAT Band	Waveno. Range (cm^{-1})
SWIR-3	5176–5193



Table 4. Definition of GOSAT/GOSAT-2 spectral fit windows (same for S and P). Windows 7 and 8 are only available for GOSAT-2.

No.	Primary target	Waveno. range (cm ⁻¹)	Considered gases
1	SIF	13170 – 13220	O ₂
2	O ₂	12930 – 13170	O ₂
3	HDO	6337 – 6410	CO ₂ , H ₂ O, HDO, CH ₄
4	CO ₂	6161 – 6297	CO ₂ , H ₂ O, HDO, CH ₄
5	CH ₄	5945 – 6135	CO ₂ , H ₂ O, HDO, CH ₄
6	CO ₂	4801 – 4907	CO ₂ , H ₂ O, HDO
7	N ₂ O	4364 – 4449	N ₂ O, H ₂ O, HDO, CH ₄
8	CO	4228 – 4328	CO, H ₂ O, HDO, CH ₄



Table 5. State vector elements and related retrieval settings. A-priori values are also used as first guess. “Fit windows” lists the spectral windows (see Tab. 4) from which the element is determined. “all” means that an element is determined from all fit windows of the specified polarisation. “each” means that a corresponding element is fitted in each fit window. A-priori values labelled as “PP” are taken from pre-processing; “est.” denotes that they have been estimated from the background signal

Element	Fit windows	A-priori	A-priori uncertainty	Comment
Gases				
co2_lay	3,4,5,6 (S&P)	PP	10.0	CO ₂ profile (5 layers), in ppm
ch4_lay	3,4,5 (S&P)	PP	0.045	CH ₄ profile (5 layers), in ppm
h2o_lay	3,4,5,6 (S&P)	PP	5.0	H ₂ O profile (5 layers), in ppm
sif_fac	1 (S&P)	0.	5.	SIF spectrum scaling factor
delta_d	3,4,5,6 (S&P)	-200.	1000.	δD profile scaling factor
n2o_scl	7 (S&P)	1.	0.1	N ₂ O profile scaling factor, only GOSAT-2
co_scl	8 (S&P)	1.	1.0	CO profile scaling factor, only GOSAT-2
Scattering parameters				
pre_sca_s	all S	0.2	1.	Layer height (pressure), S
tau_sca_0_s	all S	0.01	0.1	Optical depth, S
ang_sca_s	all S	4.0	1.	Ångström coefficient, S
pre_sca_p	all P	0.2	1.	Layer height (pressure), P
tau_sca_0_p	all P	0.01	0.1	Optical depth, P
ang_sca_p	all P	4.0	1.	Ångström coefficient, P
Polynomial coefficients (surface albedo)				
poly0	each	est.	0.01	estimated surface albedo
poly1	each	0.2	0.1	
poly2	each	0.1	0.1	not in SIF window (1)
Spectral corrections				
wav_shi	each	0.0	0.1	Wavenumber shift
wav_squ	each	0.0	0.001	Wavenumber squeeze



Table 6. Parameters of GOSAT noise model.

Fit window	s	δF	a_0	a_1	a_2	NSR range
S polarisation						
1	1.12	2.17e-03	9.369e-05	1.613e-01	-9.185e-01	0.003–0.049
2	1.07	5.50e-03	1.183e-03	2.557e-02	1.107e+00	0.003–0.047
3	1.14	3.61e-03	5.241e-04	1.251e-01	-6.776e-01	0.003–0.043
4	1.07	3.37e-03	5.480e-04	7.250e-02	3.716e-02	0.003–0.041
5	1.07	3.58e-03	8.836e-04	3.433e-02	8.853e-01	0.003–0.047
6	1.00	7.12e-03	1.680e-03	-9.060e-03	1.190e+00	0.001–0.047
P polarisation						
1	1.13	2.42e-03	5.961e-04	8.736e-02	6.867e-01	0.003–0.049
2	1.05	7.50e-03	3.177e-03	-1.109e-01	2.711e+00	0.003–0.049
3	1.21	3.17e-03	4.909e-04	1.226e-01	5.539e-02	0.003–0.037
4	1.09	3.33e-03	6.725e-04	4.661e-02	1.002e+00	0.003–0.035
5	1.04	3.58e-03	6.457e-04	5.710e-02	2.663e-01	0.003–0.039
6	1.00	6.96e-03	1.488e-03	-9.996e-04	1.262e+00	0.003–0.049



Table 7. Parameters of GOSAT-2 noise model.

Fit window	s	δF	a_0	a_1	a_2	NSR range
S polarisation						
1	0.90	3.65e-03	5.895e-04	2.314e-01	-1.524e+01	0.003–0.009
2	0.94	5.21e-03	1.143e-03	1.352e-02	4.058e+00	0.003–0.009
3	1.20	3.14e-03	3.972e-04	2.756e-01	7.753e+00	0.001–0.009
4	1.08	5.25e-03	2.491e-04	2.683e-01	-4.440e-01	0.001–0.007
5	1.06	4.04e-03	2.184e-04	4.112e-01	-2.730e+01	0.001–0.007
6	1.01	4.73e-03	6.001e-04	4.469e-01	-2.822e+01	0.001–0.011
7	1.16	7.53e-03	1.289e-03	3.984e-01	-1.377e+01	0.001–0.009
8	1.11	9.34e-03	9.305e-04	5.126e-01	-2.263e+01	0.003–0.017
P polarisation						
1	0.96	2.83e-03	8.010e-05	2.856e-01	-9.105e+00	0.003–0.017
2	0.97	6.08e-03	2.258e-03	-1.191e-01	6.365e+00	0.003–0.015
3	1.19	3.20e-03	6.571e-04	9.767e-02	1.049e+01	0.001–0.011
4	1.10	5.25e-03	3.868e-04	2.064e-01	-1.886e+00	0.001–0.009
5	1.08	4.17e-03	6.688e-05	4.935e-01	-3.445e+01	0.001–0.009
6	1.02	4.68e-03	1.181e-03	1.123e-01	1.245e+00	0.001–0.015
7	1.01	7.11e-03	1.907e-03	-3.405e-02	1.012e+01	0.003–0.015
8	1.10	9.52e-03	2.093e-03	1.632e-01	-2.418e+00	0.003–0.021



Table 8. Basic filter parameters.

Filter	Range for valid data
Good convergence	$\chi^2 \leq 2$
RSR (each fit window, S&P)	below outlier limit
Scattering layer height (S&P)	0 to 1
Ångström coefficient (S&P)	1 to 5
Scattering layer optical depth (S&P)	0 to 0.02
XCO ₂ error	0 to 2.0 ppm



Table 9. Bias filter limits.

Filter	Range for valid data
GOSAT land	-6.9 to -2.9 ppm
GOSAT water	-8.1 to -4.1 ppm
GOSAT-2 land	-4.0 to 0.0 ppm
GOSAT-2 water	-5.5 to -1.5 ppm